nature portfolio

Peer Review File

Directing Ru-based acidic oxygen evolution catalysts toward a universal dual-site pathway

Corresponding Author: Professor Chuangang Hu

This file contains all reviewer reports in order by version, followed by all author rebuttals in order by version.

Attachments originally included by the reviewers as part of their assessment can be found at the end of this file.

Version 0:

Reviewer comments:

Reviewer #1

(Remarks to the Author)
The OPM offers intrinsically superior kinetics for the anodic OER, yet its universal activation remains elusive. Although various doping strategies have recently been developed to modulate the reaction pathway, precisely controlling the OPM on a global scale is still highly difficult. This manuscript addresses this challenge in the integrated-screened Y0.1Ir0.2Ru0.7Ox by precisely regulating the Ru-Ru1 bond length and constructing locally ordered yet long-range disordered structures, thereby enabling homogeneous modulation of interatomic distances across the framework. The typical sample Y0.1Ir0.2Ru0.7Ox successfully achieves the anticipated universal OPM and extends this innovative concept to practically meaningful devices with high electrochemical performance. The data throughout the paper are substantial, the writing is rigorous, and the proposed strategy and resulting performance show a consistent and reasonable correlation. However, some descriptions do not provide entirely satisfactory explanations and certain intriguing aspects are not sufficiently discussed. I look forward to the authors refining and expanding these sections to achieve a more coherent presentation before publication in Nature communication.
1. The manuscript briefly describes that Y0.1Ir0.2Ru0.7Ox exhibits good stability in the three-electrode configuration (Supplementary Fig. 44). However, the duration of the steady-state current test appears relatively short, and the comparison with reference samples is not shown. The authors are encouraged to provide additional relevant data.
2. In Fig. 3 of the main text, the authors only present the LSV curves of the catalysts in the three-electrode setup, but commonly used comparison metrics such as turnover frequency are not included. Please provide and standardize these data for completeness.
3. In the Supplementary Information, the authors intended to present cross-sectional SEM images of membrane electrodes coated with different catalysts. However, Supplementary Fig. 46 only compares the sample with a commercially coated RuO2 catalyst. The absence of data on “the performance and macroscopic morphology of the commercial catalyst at a low loading” weakens the persuasiveness of morphology-related discussions. The manuscript should include corresponding data for the commercial catalyst under the same loading as the typical sample.
4. It is recommended to include data showing the catalyst’s stability over at least 24 h under fluctuating current and thermal start-stop voltage conditions in PEMWE, to enhance the significance of the step-current tests.
5. In Supplementary Fig. 34, the caption indicates Ir LIII-edge data, but the comparison sample is labeled as “RuO2.” Please correct this inconsistency and ensure the reliability of the data.
6. In the description related to Fig. 4 (e.g., Page 15, Lines 6-7), strengthening the connection between the *OH peak observed in FTIR, the *OH adsorption behavior discussed in MOR supplementary tests, and the elementary reaction steps analyzed in DFT calculations could significantly improve the coherence and readability of the manuscript.
7. There are additional wording and phrasing issues that need further consideration. For example, the use of “Conversely, …” to state that Ru and Ir undergo valence-state changes in different ways is somewhat semantically unclear on first reading (Page 8, line 21); likewise, words such as “indicating” appear too frequently.

Reviewer #2

(Remarks to the Author)
This manuscript presents a well-conceived study on the design of a Y0.1Ir0.2Ru0.7Ox catalyst for the acidic OER. The work

tackles a key challenge in PEMWE by aiming to guide the reaction pathway toward the kinetically favorable OPM. The combination of theoretical calculations with advanced structural and operando spectroscopic characterization (ATR-FTIR, DEMS) provides a coherent set of evidence supporting the proposed mechanism. In PEMWE, the catalyst shows excellent performance with a reduced PGM loading. The concept of lattice compression to modulate dual-site OPM activity is interesting and may provide useful insights for future catalyst design. The following suggestions are intended to further reinforce the mechanistic understanding and overall impact of the work.

1.The in situ XPS results for the Y0.1Ir0.2Ru0.7Ox catalyst provide valuable insights into the electronic stability under operating conditions. To more clearly illustrate the specific effect of Y-doping in mitigating potential-driven oxidation state changes and structural evolution, it would be helpful to include comparative in situ XPS measurements for key reference samples. Such a direct comparison would better substantiate the proposed role of Y in enhancing electronic and structural robustness.

2. While the evidence for the OPM pathway in the optimized Y-doped catalyst is convincing, the general framework linking lattice compression to OPM activity could be further supported by extending the mechanistic study. Complementary ATR-FTIR analyses on other MRuIrOx samples (e.g., SrRuIrOx and MgRuIrOx) with different Ru-Ru bond lengths would provide an opportunity to test the generality of the proposed design principle. Establishing a correlation between bond-length compression and spectroscopic OPM signatures across multiple systems would offer strong support for the proposed bond-length OPM activity relationship.

3. The manuscript attributes a part of superior mass transport properties to improved hydrophilicity and gas release behavior, which could be further clarified with quantitative evidence. Conducting high-speed video microscopy to measure O2 bubble dynamics (e.g., bubble residence time and departure diameter) under operando conditions, combined with contact angle and surface energy measurements, would help establish a more quantitative link between the catalyst's mesostructure, wettability, and high-current performance.

4. To further explore the proposed OPM pathway, it may be informative to conduct ring disk electrode measurements. Examining the potential-dependent yield of H2O2, which is a possible product from the *OOH intermediate in the AEM pathway but not typically associated with the OPM could provide additional mechanistic insight. If measurable differences are observed between Y0.1Ir0.2Ru0.7Ox and reference catalysts, this would offer useful complementary evidence regarding the dominant reaction route.

5. The stability tests in PEMWE are a major strength of the study. To further understand the degradation behavior and confirm the stabilizing role of Y, additional post-reaction analyses of the MEA would be useful (e.g., SEM, EDS, XPS etc.).

6. It may be informative to further explore the reaction kinetics through extended electrochemical impedance spectroscopy measurements over a wider potential range (e.g.,1.3-1.6 V vs. RHE). Fitting the data with an appropriate equivalent circuit could, if feasible, help identify features related to intermediate adsorption and desorption processes. Such exploratory analysis might provide additional insight into the kinetic characteristics of the O-O coupling step on the Y0.1Ir0.2Ru0.7Ox catalyst.

Reviewer #3

(Remarks to the Author)

The manuscript entitled “Directing acidic oxygen evolution catalysts toward a universal dual-site pathway” reports the design of $Y_{0.1}Ir_{0.2}Ru_{0.7}O_x$ catalysts that enable an oxide path mechanism (OPM) for acidic oxygen evolution. Through lattice-distance modulation, structural disorder engineering, and operando spectroscopy, the authors claim to achieve pervasive dual-site activation. The topic is highly relevant to the electrocatalysis and hydrogen energy communities, and the study combines advanced experimental and theoretical approaches.

However, the novelty of the material is compromised by other Ir- and Ru-based systems in which OPM-type properties have already been demonstrated. More specifically, in a recent and very similar work by the same authors (DOI: 10.1002/adfm.202515512), which is not cited in the present manuscript, a Ru_2IrO_x-based catalyst exhibiting OPM characteristics and comparable performance (~3 A cm^{-2} at around 1.8 V) was reported. Nevertheless, the 3 A cm^{-2} @ 2800 h achieved here, with loadings of 0.4 mgcat cm^{-2} for the anode and 0.5 mgcat cm^{-2} for the cathode in a PEM configuration, is indeed quite impressive. The latter aspect is probably relevant enough to deserve the opportunity for revision; however, my major corrections and comments should be carefully addressed.

– The authors mention that “A two-step ion etching process during XPS revealed an ~10% increase in the relative content of Y, indicating that Y is more enriched in the inner layers of the structure.” However, the etching procedure itself is not described, which raises concerns regarding transparency and reproducibility. Moreover, this omission casts doubt on the chemical stability of the material. Was all the characterization and activity testing performed on the etched material? Did the authors study the material without the etching process?

– The BET surface area and pore size distribution (Fig. S25) are only reported for one sample; the effect of Y incorporation on porosity compared to $Ir_{0.2}Ru_{0.8}O_x$ is not shown.

– The claim that Y induces charge redistribution (“Y promotes Ir to act as a negative charge centre”) is derived solely from Bader analysis and lacks experimental validation. Shifts in the XANES edge position would provide direct evidence and should be included.

- The Tafel slope and overpotential are claimed to be “intrinsic,” but uncompensated resistance (iR) correction details are lacking. EIS Nyquist plots (not just Bode) should be shown to confirm the high-frequency resistance values used.

- The durability test claims (2800 h @ 3 A cm^{-2}) are extremely strong; however, no post-mortem structural analysis (TEM/XPS/EXAFS) after this test is shown in the main text, only after 100 h (Fig. S44). This raises questions about possible

microstructural evolution or Y leaching over thousands of hours.

– The ECSA normalization (Figs. S40–S41) is based on double-layer capacitance, which may not accurately reflect the number of active sites in disordered oxides. The authors should estimate ECSA by alternative methods such as Ru redox charge integration or underpotential deposition.

– The signals in the FTIR spectra correspond to bands, not discrete peaks. The authors should provide the exact wavenumber positions of all relevant bands in the figures so that the discussion can be followed more precisely.

– I am highly skeptical about the interpretation of the FTIR bands. The spectra in Figures 4c and 4d show no clear or significant differences. The authors assign the band at approximately 1230 cm^{-1} to –OO* species; however, the cited reference (Ref. 38), which forms the basis for this assignment, actually attributes this band to Si–O–Si vibrations, while the –OO* feature is reported closer to 1200 cm^{-1}. In this region, the Y-free sample displays a higher band intensity, which could simply arise from greater Si exposure on the surface—perhaps due to a lower catalyst loading. This lower loading could also explain the weaker signal at ~1070 cm^{-1} in the Y-free sample, which the authors attribute to bridging oxygen species. Hence, more intense and clearly distinguishable FTIR features are needed before the claim of OPM promotion in the Y-containing catalyst can be considered reliable.

– Why does the 1070 cm^{-1} band shift with potential? The manuscript should explain this potential-dependent behaviour.

– The authors should carefully verify the consistency between the labels in Figure 4 and those mentioned in the text, as some appear mismatched.

– Regarding the DEMS experiments, the authors state that “the intensity of $^{36}O_2$ is unusually high.” I fully agree; however, further clarification is needed. Was Ar used to deoxygenate the electrolyte? Ar^+ produces a signal at m/z = 36, which could artificially elevate the baseline. Did the authors perform any calibration or blank tests prior to these measurements?

– Finally, the manuscript concludes that “almost all active sites follow the OPM pathway.” The current data do not allow quantification of the fraction of OPM-active sites. To support such a strong statement, additional operando experiments—such as O K-edge XAS, Raman under bias, or isotope-dependent Tafel analyses—would be necessary.

Reviewer #4

(Remarks to the Author)
The manuscript aims to develop a universal design strategy for acidic OER catalysts following the OPM. The authors report a designed composition, Y0.1Ir0.2Ru0.7Ox, which achieves 3A cm–2 at 1.75 V in PEM water electrolysis and remains stability for 2800 h with a degradation rate of 0.0625 mV h-1. The study contains interesting results, but several substantive issues must be addressed before the manuscript can be considered for publication.

Major comments:
1. Inconsistency between text and figures. There is a serious inconsistency between the text and the figures in the Reaction pathway elucidation section. Figs. 4i and 4h are referenced in the text (page 14, line 7; page 15, line 1), but they are missing from the manuscript. Please check and correct the figure numbering.
2. The authors conclude that Y0.1Ir0.2Ru0.7Ox follows OPM while Ir0.2Ru0.8Ox follows AEM. However, LOM pathways cannot be fully excluded on the basis of the current evidence. I recommend a chemical-probe test (e.g., with and without TMA) or other established isotope/probe experiments to distinguish OPM from LOM unambiguously. Also, the Raman/IR wavenumber assigned to OOH (reported here) differs from values reported in the literature (e.g., ~986 cm^{-1}, Nat. Catal., 2021, 12, 1012–1023); please reconcile or justify this discrepancy.
3. The DFT-guided microscopic structural design section lacks logical coherence with later sections. The synthesis, characterization and electrochemical performance of various samples (such as Y0.1Ir0.2Ru0.7Ox and Ir0.2Ru0.8Ox, et al.) are described later in the manuscript, yet their electrochemical data (e.g., YRuIrOx and RuIrOx) already appear in earlier sections (Fig. 1e, Supplementary Figs. 2–4 and 7). In addition, the overpotential of YRuIrOx and Y0.1Ir0.2Ru0.7Ox differ noticeably. Are these samples identical and prepared via the same synthesis route? Please clarify the sample naming and experimental sequence to avoid confusion.
4. The hypothesis states that densely packed dual sites with short Ru–Ru_1 bonds favor OPM. However, Fig. 1f presents step energy barriers only for Y0.1Ir0.2Ru0.7Ox. To support the claim convincingly, perform equivalent calculations for other samples with similar Ru–Ru_1 distances (e.g., RuIrOx, SrRuIrOx; see Figs. 1c and 1e). Comparative DFT results will demonstrate whether the short Ru–Ru_1 distance itself is the decisive factor.
5. The respective roles of Ir and Ru in facilitating OPM are not clearly declared. Specify which atomic sites were modeled as active centers in the calculations and discuss how Ru and Ir individually contribute to the proposed OPM pathway.
6. Potential dissolution of Y and related surface evolution in acid appear overlooked. Does Y0.1Ir0.2Ru0.7Ox retain the nominal atomic ratio after OER test? Characterizations should be employed before and after stability test, such as ICP-MS, SEM, TEM and EDS.
7. The statements “exceptional operational stability (>2,800 h @ 3 A cm-2)” (Abstract) and “exceptional stability for 2,800 h” (p. 12) are overstated given the reported potential degradation (≈175 mV). Remove the word “exceptional” or temper the language and explicitly report the absolute potential increase (175 mV) and the degradation rate (0.0625 mV h-1) so readers

can judge practical relevance.
8. The title claims a “universal design strategy,” yet the data focus on Ru/Ir-based systems. Either provide supporting results across multiple catalyst families or narrow the title (for example, incorporate “Ru-based catalysts” into the title).
9. The rationale for selecting Y, Sr, Sc and Mg should be clearly discussed. Explain why these elements were chosen over other possible dopants (electronic properties, ionic size, stability, prior literature precedents), and connect the choice to the mechanistic and structural design principles.
10. Pourbaix diagrams appear inconsistent or incomplete (Fig. 1g). Y and Ir species appear missing across the Pourbaix regions shown. Explain the meaning of the blue-filled regions and the mesh region in the figure. Verify the Pourbaix calculations and provide more detailed description (calculation conditions, concentration, pH range, potential range). Also check Fig. S20a for consistency.
11. Fig. S22 indicates phase separation of Ir from Ru oxides. Discuss possible origins and implications for activity/stability.
12. Based on the XRD analysis (Fig. S24c), is the sample a mixture of RuO2/IrO2 or a Y-Ru-Ir-O compound? The XRD pattern of Ir0.2Ru0.8Ox should be given for comparison.
13. The presence of Y reportedly shortens the Ru–Ru bond but lengthens the Ru–O bond. This appears contradictory from a bonding perspective — please explain the structural/chemical origin of this observation and, if possible, provide additional analyses to reconcile these trends.
14. Y content values are missing in Fig. 2g.
15. Update the comparison in the inset of Fig. 3f and Table 1 to include more recent Ir- and Ru-based OER catalysts published in high-impact journals to ensure a current and fair performance comparison.

Minor comments:
1. Supplementary Figure 13a shows that Sr also bridge adsorbs *OH and participates reaction. Does this structure influence the early intermediates such as *OH energy barriers, or still follow OPM?
2. The potential window of Pourbaix diagram in Fig. 1g is of –0.5~1.5 V differs from those of Ir0.2Ru0.8Ox and Ru (Supplementary Fig. 20). A higher potential of Pourbaix diagram should be performed to elucidate the thermodynamic stability of Y0.1Ir0.2Ru0.7Ox, because practical application may operate at higher voltages.
3. References 29 and 30 do not mention the statement “…act as a negative charge centre, protecting Ru from overoxidation” (Page 8 line 15). Please verify and correct this citation.
4. The method used to calculate the S-number and the comparison with reported Ir- and Ru-based catalysts should be added for completeness.
5. The statement “…(0.1 mgIr cm-2 and 0.3 mgIr cm-2)…” on page 16 line 11 appears to be incorrect. Please revise accordingly.
6. The method for evaluating PEMWE activity in Fig. 3c should be described in detail, including electrochemical measurements and flow rates. In addition, the active area for evaluating activity and stability in PEMWE should also be declared.

Version 1:

Reviewer comments:

Reviewer #1

(Remarks to the Author)
I am satisfied with the revision, and it can be accepted at the present state.

Reviewer #2

(Remarks to the Author)
The authors have addressed all my concerns. I think the revised manuscript could be accepted in this journal now.

Reviewer #3

(Remarks to the Author)
The technical concerns have been fully and well resolved, and while the material overlap with previous work is notable, the superior performance demonstrated here provides sufficient impact for publication in Nature Communications.

Reviewer #4

(Remarks to the Author)
Please see the attachment.

Version 2:

Reviewer comments:

Reviewer #4

(Remarks to the Author)
The authors have further addressed my comments; however, the discussion based on the Ru Pourbaix diagram to evaluate the thermodynamic stability of Y0.1Ir0.2Ru0.7Ox remains inappropriate. In particular, some statements are misleading. A Pourbaix diagram is fundamentally used to assess thermodynamic stability and possible phase stability domains under electrochemical conditions, not catalytic activity. Therefore, the statement that “Y2O3 themself exhibits negligible intrinsic catalytic activity toward OER relative to the Y0.1Ir0.2Ru0.7Ox catalyst under typical electrochemical operating conditions.” is conceptually incorrect in this context. Thermodynamic stability analysis cannot be used to justify catalytic activity comparisons.
More importantly, the stability of Y-containing species is not properly addressed. Y2O3 (or Y species in the oxide lattice) may undergo dissolution or phase instability under operating OER conditions, which could significantly affect catalyst durability. This aspect appears to be overlooked.
Accordingly, the authors are encouraged to construct and analyze the Pourbaix diagram of Y0.1Ir0.2Ru0.7Ox, rather than relying solely on the Ru Pourbaix diagram, which does not adequately represent the multicomponent system.

Version 3:

Reviewer comments:

Reviewer #4

(Remarks to the Author)
I appreciate the authors' efforts in revising the manuscript. The removal of the misleading statements regarding catalytic activity, together with the inclusion of a multicomponent Pourbaix analysis that explicitly considers Y-containing phases, has substantially improved the discussion and addressed my previous concerns. Since the authors still keep the initial Pourbaix analysis in Fig. 1g, I believe, that several aspects of the interpretation would benefit from more cautious wording to ensure that the conclusions remain fully consistent with the scope and limitations of the Pourbaix analysis.
According to Supplementary Figure 20, the thermodynamically stable phase under OER-relevant conditions is predicted to be Y2Ir2O7, rather than the synthesized Y0.1Ir0.2Ru0.7Ox, suggesting that the catalyst is thermodynamically metastable. Therefore, the statement that "Y incorporation does not introduce a preferential thermodynamic driving force for Y dissolution" would benefit from more careful qualification. The Pourbaix analysis identifies the equilibrium phase assemblage with the lowest Gibbs free energy but does not demonstrate that Y remains incorporated within the original catalyst lattice during operation. Likewise, the predicted equilibrium of Y2Ir2O7 and RuO4 indicates that phase reconstruction is thermodynamically favorable. Accordingly, the conclusions regarding catalyst durability should continue to rely primarily on the experimental stability results, with the Pourbaix analysis providing qualitative thermodynamic insight.
Moreover, please make sure RuO4 in Supplementary Figure 20 is solid species since RuO4 appears as dissolved species in Fig. 1g.
In addition, I suggest a minor revision to the description of Fig. 1g. Based on the computational methodology and the authors' explanation, Fig. 1g represents a Ru-centered Pourbaix analysis of Ru-related phases under different chemical environments, rather than a true Pourbaix diagram of Y0.1Ir0.2Ru0.7Ox.
If the authors would like to keep Fig. 1g as it is, revising the figure caption and corresponding discussion to reflect this distinction would improve consistency with the methodology and avoid confusion with the multicomponent Pourbaix analysis presented in Supplementary Figure 20. These minor clarifications would further strengthen the scientific rigor of the manuscript.

Response to Reviewers

First, please allow us to express our sincere gratitude to all the Reviewers who have provided valuable comments on this manuscript. After receiving the Reviewers' feedback, we have done our best to address each point and clarify our perspectives. We have also included the revised portions of the manuscript (marked in blue) in the resubmission. We would like to express our appreciation once again.

Reviewer#1

The OPM offers intrinsically superior kinetics for the anodic OER, yet its universal activation remains elusive. Although various doping strategies have recently been developed to modulate the reaction pathway, precisely controlling the OPM on a global scale is still highly difficult. This manuscript addresses this challenge in the integrated-screened $Y_{0.1}Ir_{0.2}Ru_{0.7}O_x$ by precisely regulating the Ru-Ru$_1$ bond length and constructing locally ordered yet long-range disordered structures, thereby enabling homogeneous modulation of interatomic distances across the framework. The typical sample $Y_{0.1}Ir_{0.2}Ru_{0.7}O_x$ successfully achieves the anticipated universal OPM and extends this innovative concept to practically meaningful devices with high electrochemical performance. The data throughout the paper are substantial, the writing is rigorous, and the proposed strategy and resulting performance show a consistent and reasonable correlation. However, some descriptions do not provide entirely satisfactory explanations and certain intriguing aspects are not sufficiently discussed. I look forward to the authors refining and expanding these sections to achieve a more coherent presentation before publication in Nature communication.

We sincerely thank the Reviewer for reading our manuscript and providing his/her scientific feedback. We have made revisions to the manuscript based on the suggestions as provided.

Comment 1:

The manuscript briefly describes that $Y_{0.1}Ir_{0.2}Ru_{0.7}O_x$ exhibits good stability in the three-electrode configuration (Supplementary Fig. 44). However, the duration of the steady-state current test appears relatively short, and the comparison with reference samples is not shown. The authors are encouraged to provide additional relevant data.

Response: We thank the Reviewer for his/her insightful comment. Accordingly, we conducted an extended 500 h three-electrode stability test, yielding a decay rate of 12.3

μV h^{-1}, to replace the original data in **Supplementary Fig. 47** in the revised Supplementary Information.

Comment 2:

In Fig. 3 of the main text, the authors only present the LSV curves of the catalysts in the three-electrode setup, but commonly used comparison metrics such as turnover frequency are not included. Please provide and standardize these data for completeness.

Response: We sincerely thank the Reviewer for providing his/her scientific feedback. We fully agree that the turnover frequency (TOF) is highly valuable for evaluating the intrinsic activity of active sites in OER catalysts. Following the Reviewer's suggestion, we have now provided TOF estimates based on the specific surface area derived from the double-layer capacitance.

$$TOF_{C_{dl}} = \frac{j}{n \times F \times N_{active\ sites\ density}}$$

$$N_{active\ sites\ density} = \frac{atom\ number}{(a \times c) \times \sin\gamma}$$

To provide information with meaningful comparability, we need to made the following assumptions: (i) all surface planes are rutile-RuO_2 (110); (ii) The supplemented BET data (Supplementary Figure 25) were used as the source for the specific surface area values. The related information has been added to the revised Supplementary Information (**Supplementary Figure 41**).

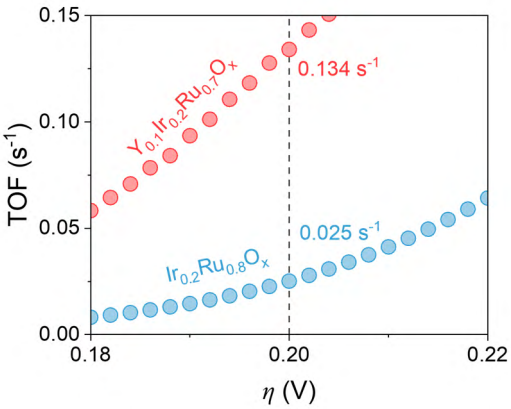

Supplementary Figure 41. The TOF values of $Y_{0.1}Ir_{0.2}Ru_{0.7}O_x$ and $Ir_{0.2}Ru_{0.8}O_x$ based on BET results.

Comment 3:

In the Supplementary Information, the authors intended to present cross-sectional SEM

images of membrane electrodes coated with different catalysts. However, Supplementary Fig. 46 only compares the sample with a commercially coated RuO_2 catalyst. The absence of data on "the performance and macroscopic morphology of the commercial catalyst at a low loading" weakens the persuasiveness of morphology-related discussions. The manuscript should include corresponding data for the commercial catalyst under the same loading as the typical sample.

Response: We thank the Reviewer for his/her valuable comments. To better illustrate the thickness and uniformity of commercial crystalline RuO_2 loaded on the MEA at low loadings, we have added cross-sectional SEM images of a Com-RuO_2 MEA at a loading of 0.4 mg cm^{-2} as supplementary data. At the same loading, the lamellar $Y_{0.1}Ir_{0.2}Ru_{0.7}O_x$ forms a thinner catalyst layer than Com- RuO_2, and it is also thinner than Com-RuO_2 at a typical commercial loading of 1.0 mg cm^{-2}. Owing to its particulate nature, Com-RuO_2 exhibits rapid thickness buildup and expansion with increasing loading, which hinders mass transport and reduces precious-metal utilization. In contrast, the thinner $Y_{0.1}Ir_{0.2}Ru_{0.7}O_x$ layer more readily delivers improved mass-transport characteristics at low loadings. The updated **Supplementary Figure 49** has been incorporated into the revised manuscript.

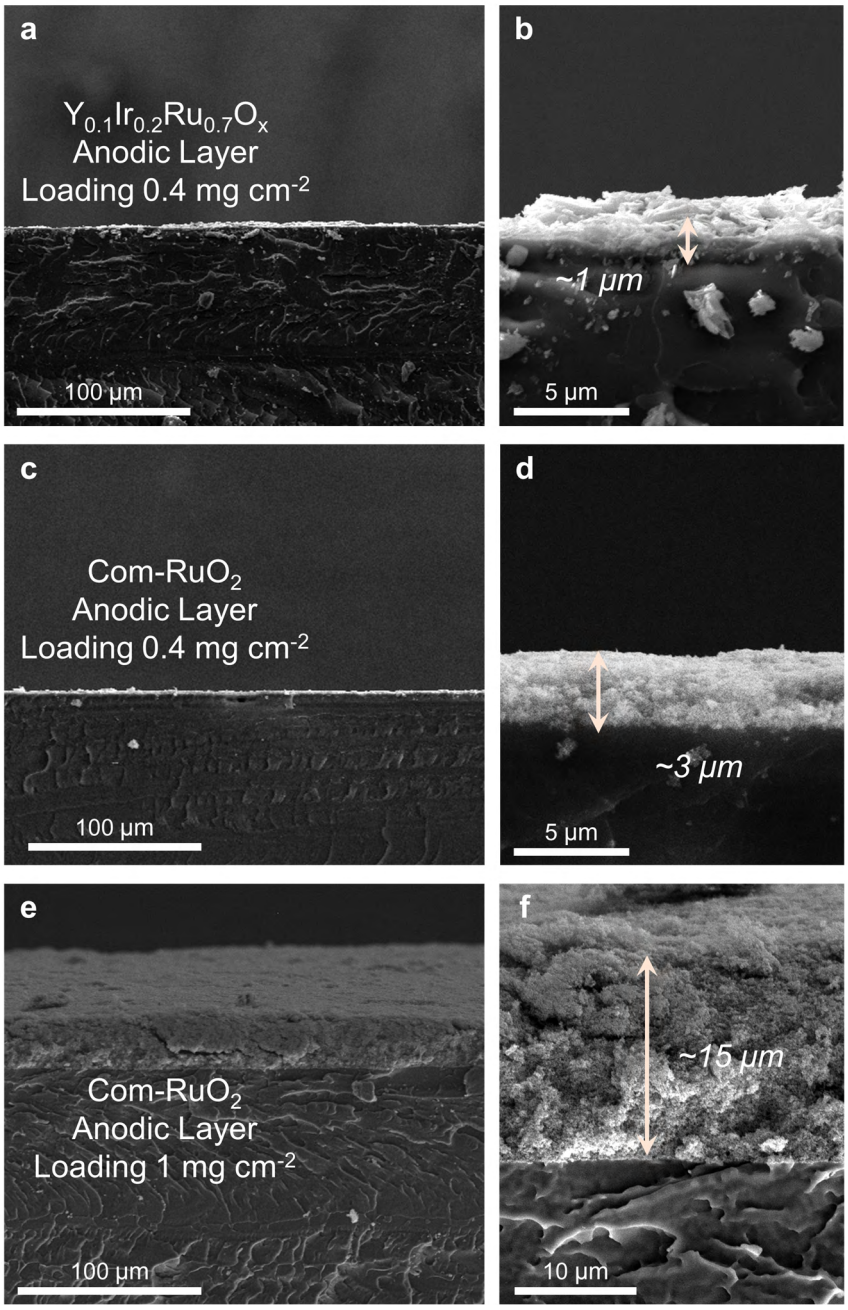

Supplementary Figure 49. Cross-sectional MEA interface images loaded with (a, b) 0.4 mg cm^{-2} of $Y_{0.1}Ir_{0.2}Ru_{0.7}O_x$, (c, d) 0.4 mg cm^{-2} of Com-RuO_2, and (e, f) 1.0 mg cm^{-2} of Com-RuO_2 together with their corresponding magnified SEM micrographs.

Comment 4:

It is recommended to include data showing the catalyst's stability over at least 24 h under fluctuating current and thermal start-stop voltage conditions in PEMWE, to enhance the significance of the step-current tests.

Response: We appreciate the insightful suggestion from the Reviewer. We fully agree that the dynamic-performance characteristics under fluctuating operating conditions are

crucial for evaluating the long-term durability of MEAs in PEMWE systems. Introducing square-wave accelerated degradation tests (ADT) has become an important approach in both PEMFC and PEMWE fields for assessing catalyst stability under frequently changing redox environments, including frequent thermal start-stop and chemical environment change. As shown, we conducted square-wave ADT measurements on the anode catalyst ($Y_{0.1}Ir_{0.2}Ru_{0.7}O_x$) under a square-wave load with an amplitude of 2 A cm^{-2} and a frequency of 1/30 Hz.

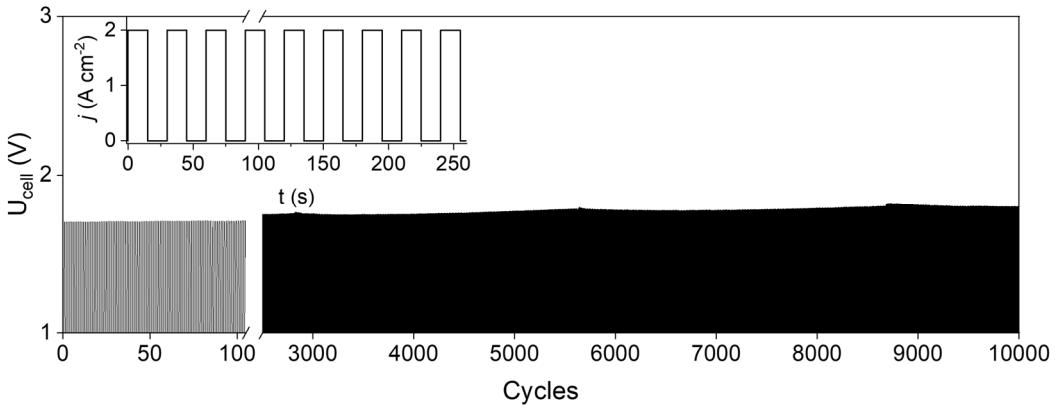

Supplementary Figure 55. U_{cell}-cycle profile of $Y_{0.1}Ir_{0.2}Ru_{0.7}O_x$ under square-wave ADT operation. Inset: Applied square-wave ADT waveform.

After 10,000 square-wave cycles, the anode with a loading of 0.4 mg cm^{-2} $Y_{0.1}Ir_{0.2}Ru_{0.7}O_x$ exhibited an average degradation rate of 8 μV $cycle^{-1}$. Considering the membrane degradation induced by the frequently changing chemical environment near the proton-exchange membrane in pure-water systems, as well as the accelerated deterioration of other PEMWE components such as the gas-diffusion layer under square-wave operation, $Y_{0.1}Ir_{0.2}Ru_{0.7}O_x$ indeed demonstrates robust long-term performance under dynamically fluctuating conditions. This observation is also consistent with the impressive stability of $Y_{0.1}Ir_{0.2}Ru_{0.7}O_x$ under step-potential operation shown in Fig. 3f. The above information has been added to the revised manuscript. (**Supplementary Figure 57**).

Comment 5:

In Supplementary Fig. 34, the caption indicates Ir L_{III}-edge data, but the comparison sample is labelled as "RuO_2." Please correct this inconsistency and ensure the reliability of the data.

Response: We sincerely appreciate the Reviewer for pointing out our oversight. The

incorrect labels in the XAFS-related figure captions have now been thoroughly re-checked and corrected.

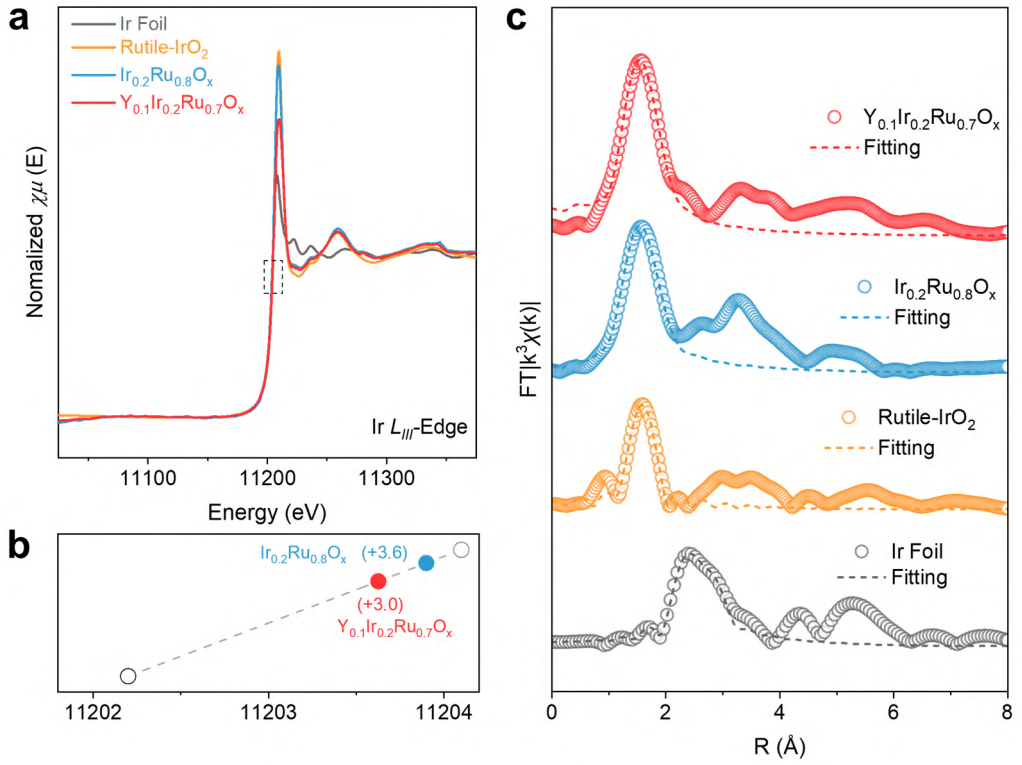

Supplementary Figure 34. Ir L_{III}-edge XAFS data. (a) Normalized spectra, (b) valence-state assignment of Ir, and (c) R-space profile.

Comment 6:

In the description related to Fig. 4 (e.g., Page 15, Lines 6-7), strengthening the connection between the *OH peak observed in FTIR, the *OH adsorption behaviour discussed in MOR supplementary tests, and the elementary reaction steps analysed in DFT calculations could significantly improve the coherence and readability of the manuscript.

Response: We thank the Reviewer for his/her helpful comments. In the initial Supplementary Information, we introduced MOR as a semi-quantitative descriptor to reflect the affinity toward OH intermediates. To further clarify and strengthen this discussion, we have added a more detailed explanation of the MOR-related information following **Supplementary Figure 73** in the revised manuscript.

Comment 7:

There are additional wording and phrasing issues that need further consideration. For example, the use of "Conversely, …" to state that Ru and Ir undergo valence-state changes in different ways is somewhat semantically unclear on first reading (Page 8,

line 21); likewise, words such as “indicating” appear too frequently.

Response: We thank the Reviewer for his/her thoughtful guidance. The inappropriate wording has been carefully identified and revised in the upgraded version (**Page 8, Line 21**).

Reviewer#2

This manuscript presents a well-conceived study on the design of a Y0.1Ir0.2Ru0.7Ox catalyst for the acidic OER. The work tackles a key challenge in PEMWE by aiming to guide the reaction pathway toward the kinetically favourable OPM. The combination of theoretical calculations with advanced structural and operando spectroscopic characterization (ATR-FTIR, DEMS) provides a coherent set of evidence supporting the proposed mechanism. In PEMWE, the catalyst shows excellent performance with a reduced PGM loading. The concept of lattice compression to modulate dual-site OPM activity is interesting and may provide useful insights for future catalyst design. The following suggestions are intended to further reinforce the mechanistic understanding and overall impact of the work.

We appreciate the Reviewer’s recognition of the content of our manuscript and the valuable feedback. Based on the suggestions, we have made the following revisions to the manuscript and Supplementary Information.

Comment 1:

The in situ XPS results for the $Y_{0.1}Ir_{0.2}Ru_{0.7}O_x$ catalyst provide valuable insights into the electronic stability under operating conditions. To more clearly illustrate the specific effect of Y-doping in mitigating potential-driven oxidation state changes and structural evolution, it would be helpful to include comparative in situ XPS measurements for key reference samples. Such a direct comparison would better substantiate the proposed role of Y in enhancing electronic and structural robustness.

Response: We thank the Reviewer for the constructive suggestion. According to the Reviewer’s comments, we designed an analogous experimental approach to examine whether the Y-free $Ir_{0.2}Ru_{0.8}O_x$ is more prone to valence-state shifts. Following a protocol comparable to that used in operando XPS studies, we investigated potential-dependent changes over the range of 0.8-1.6 V *vs.* RHE. No obvious shifts are observed in the XPS spectra of either $4f_{7/2}$ or Ru $3d_{5/2}$ after applying the additional potential (**Figure. R1**).

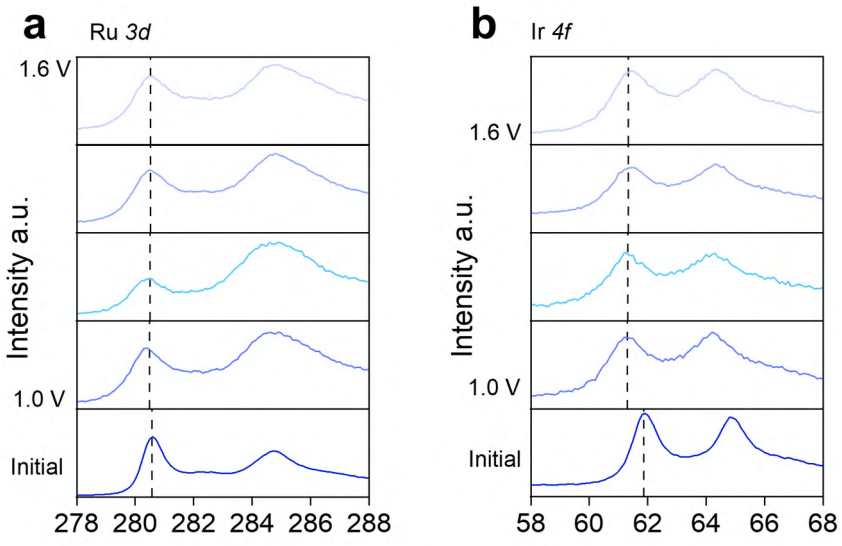

Figure. R1 Potential-programmed XPS spectra of the Y-free $Ir_{0.2}Ru_{0.8}O_x$ catalyst. (a) Ru *3d* and (b) Ir *4f* core-level spectra collected after electrochemical pre-conditioning at different applied potentials (1.0-1.6 V *vs.* RHE).

Comment 2:

While the evidence for the OPM pathway in the optimized Y-doped catalyst is convincing, the general framework linking lattice compression to OPM activity could be further supported by extending the mechanistic study. Complementary ATR-FTIR analyses on other $MRuIrO_x$ samples (e.g., $SrRuIrO_x$ and $MgRuIrO_x$) with different Ru-Ru bond lengths would provide an opportunity to test the generality of the proposed design principle. Establishing a correlation between bond-length compression and spectroscopic OPM signatures across multiple systems would offer strong support for the proposed bond-length OPM activity relationship.

Response: We thanks the Reviewer for the insightful comments. As suggested, the ATR-FTIR data of $Sr_{0.1}Ir_{0.2}Ru_{0.7}O_x$ and $Mg_{0.1}Ir_{0.2}Ru_{0.7}O_x$ have been provided to the revised manuscript. Further analysis of the additional FTIR results shows that $Sr_{0.1}Ir_{0.2}Ru_{0.7}O_x$ exhibits characteristic -OO* and -OO*- features in the fingerprint region, indicating that $Sr_{0.1}Ir_{0.2}Ru_{0.7}O_x$ follows a high fraction of the OPM pathway, similar to the that of $Y_{0.1}Ir_{0.2}Ru_{0.7}O_x$. In contrast, $Mg_{0.1}Ir_{0.2}Ru_{0.7}O_x$ exhibits a relatively larger calculated Ru-Ru_1 length, indicating the simultaneous occurrence of both the AEM and OPM pathways.

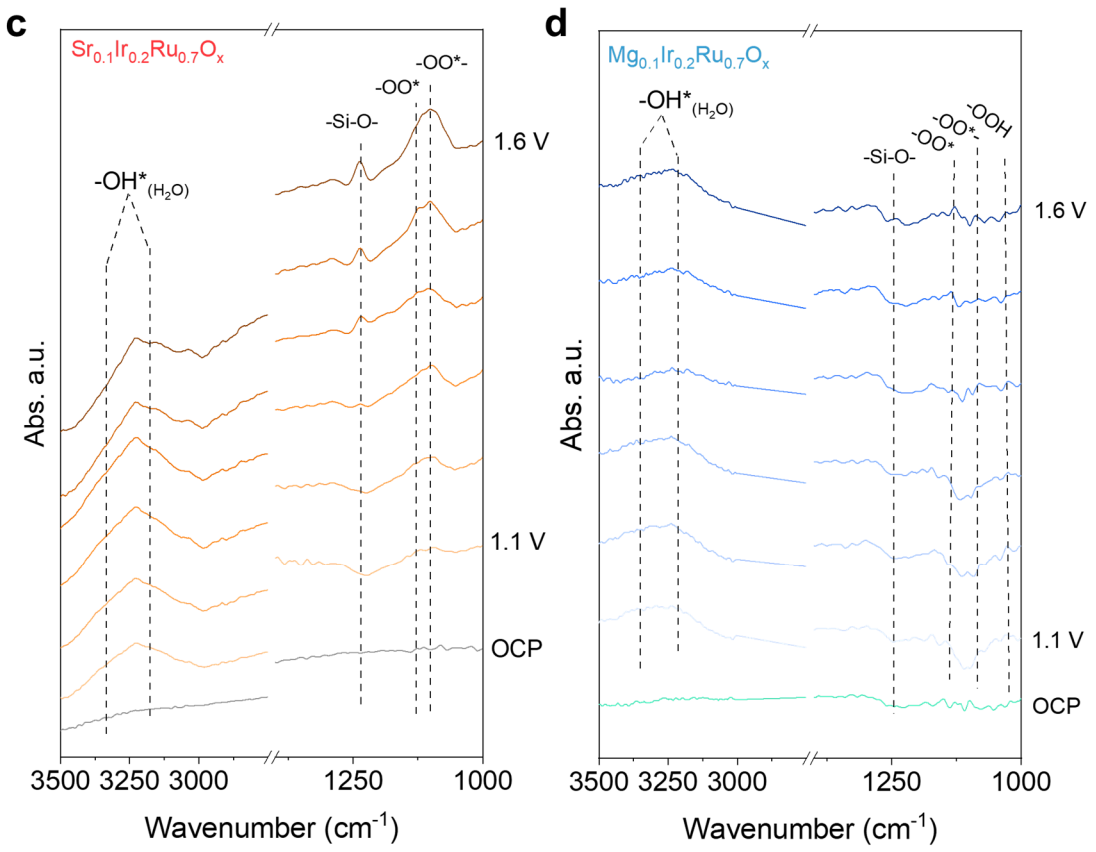

Supplementary Figure 71. ATR-FTIR spectra for (c) $Sr_{0.1}Ir_{0.2}Ru_{0.7}O_x$ and (d) $Mg_{0.1}Ir_{0.2}Ru_{0.7}O_x$. The testing process has been provided in the method section.

Comment 3:

The manuscript attributes a part of superior mass transport properties to improved hydrophilicity and gas release behaviour, which could be further clarified with quantitative evidence. Conducting high-speed video microscopy to measure O_2 bubble dynamics (e.g., bubble residence time and departure diameter) under operando conditions, combined with contact angle and surface energy measurements, would help establish a more quantitative link between the catalyst's mesostructured, wettability, and high-current performance.

Response: We thank the Reviewer for the constructive suggestion. We agree that operando high-speed visualization of bubble behaviour (e.g., residence time and departure diameter) would provide valuable insights into interfacial mass-transport processes. In the current manuscript, the discussion of hydrophilicity and gas-release behaviour is limited. Herein, we intentionally included static contact-angle measurements (Supplementary Fig. 51). Compared with the non-templated

$Y_{0.1}Ir_{0.2}Ru_{0.7}O_x$, the static contact-angle results indicate a lower contact angle and improved surface wettability, which is sufficient to support the limited qualitative statements made in the revised manuscript (**Page 11, Line 12**). This comparison is intended to highlight the influence of the synthesis methodology rather than isolate the effect of Y incorporation, as the introduction of Y is not expected to induce a substantial change in macroscopic wettability (*Bubbles, Drops, and Particles*, 2005). See Supplementary Fig. 51 for the related revisions in the revised Supplementary Information.

Comment 4:

To further explore the proposed OPM pathway, it may be informative to conduct ring disk electrode measurements. Examining the potential-dependent yield of H_2O_2, which is a possible product from the *OOH intermediate in the AEM pathway but not typically associated with the OPM could provide additional mechanistic insight. If measurable differences are observed between $Y_{0.1}Ir_{0.2}Ru_{0.7}O_x$ and reference catalysts, this would offer useful complementary evidence regarding the dominant reaction route.

Response: We appreciate the Reviewer's support in improving the manuscript. This comment provides new guidance for deepening the kinetic investigation into the OER pathways realized by $Y_{0.1}Ir_{0.2}Ru_{0.7}O_x$. As suggested, we have re-examined the ring-electrode behaviour during LSV measurements in the potential range of 1.3-1.5 V *vs.* RHE and added the results to the revised Supporting Information as Supplementary Figure 74. As shown, $Ir_{0.2}Ru_{0.8}O_x$ previously demonstrated to correlate strongly with the AEM pathway, exhibits noticeable fluctuations in the ring current in the region where OER proceeds efficiently, accompanied by pronounced fluctuations in the disk current. According to the literature (*J. Electroanal. Chem.,* 2014, 728, 102, *Science*, 2016, 353, 1011) and our DFT calculations (Supplementary Figure 19), the formation of -OOH is the typical rate-determining step for $Ir_{0.2}Ru_{0.8}O_x$; thus, the rapid formation-consumption dynamics of this key intermediate lead to an unstable environment that manifests as ring-current fluctuations.

In contrast, for $Y_{0.1}Ir_{0.2}Ru_{0.7}O_x$, -OOH species that are marginalized, desorbed, or do not participate directly in the reaction can instead form more complete Pt-affinitive reduced products, appearing as negative currents at the ring electrode. The information obtained from the RRDE measurements is therefore consistent with the ATR-FTIRAS conclusions presented in the manuscript (Fig. 4c, d). Specifically, $Ir_{0.2}Ru_{0.8}O_x$ shows

clear spectroscopic signatures of transient -OOH intermediates, whereas -OOH signals are not observed for $Y_{0.1}Ir_{0.2}Ru_{0.7}O_x$. The RRDE results support the interpretation that these marginalized -OOH intermediates dissipate and desorb as other highly oxidized species (e.g., HO_2), and thus do not appear in the spectroscopic measurements.

The corresponding explanations and Figure have been added to the revised manuscript (**Page 16, Line 8 and Supplementary Figure 76**).

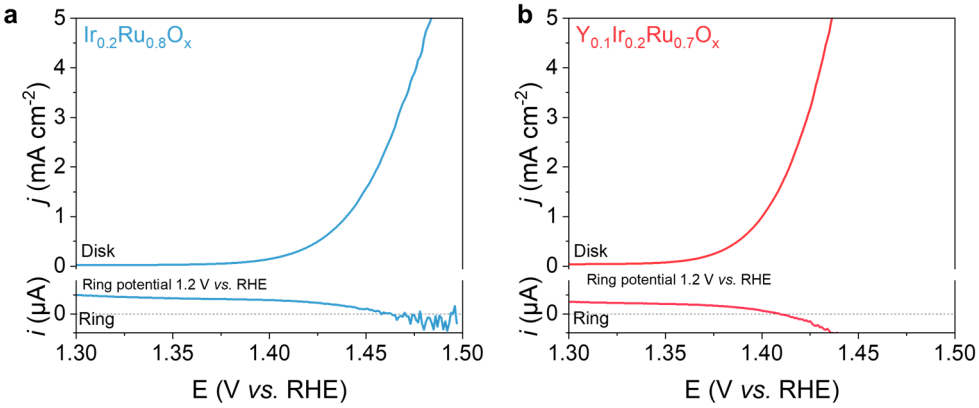

Supplementary Figure 76. Comparison of ring and disk electrode currents(a) for $Ir_{0.2}Ru_{0.8}O_x$ and (b) $Y_{0.1}Ir_{0.2}Ru_{0.7}O_x$ during the LSV measurements.

Comment 5:

The stability tests in PEMWE are a major strength of the study. To further understand the degradation behaviour and confirm the stabilizing role of Y, additional post-reaction analyses of the MEA would be useful (e.g., SEM, EDS, XPS etc.).

Response: We thank the Reviewer for his/her attention to details. We have supplemented the manuscript with SEM, EDS, and XPS characterizations of the MEA after reaction.

(i) SEM & SEM-EDS

The MEA with $Y_{0.1}Ir_{0.2}Ru_{0.7}O_x$ as the anode catalyst still maintained its original layered structure and thin catalytic layer thickness (~1 μm) after 2800 h of reaction. It can also be clearly seen from EDS images and energy spectrum conclusions that no obvious redistribution or segregation of Y, Ir, or Ru from $Y_{0.1}Ir_{0.2}Ru_{0.7}O_x$ is observed at the spatial resolution of SEM-EDS.

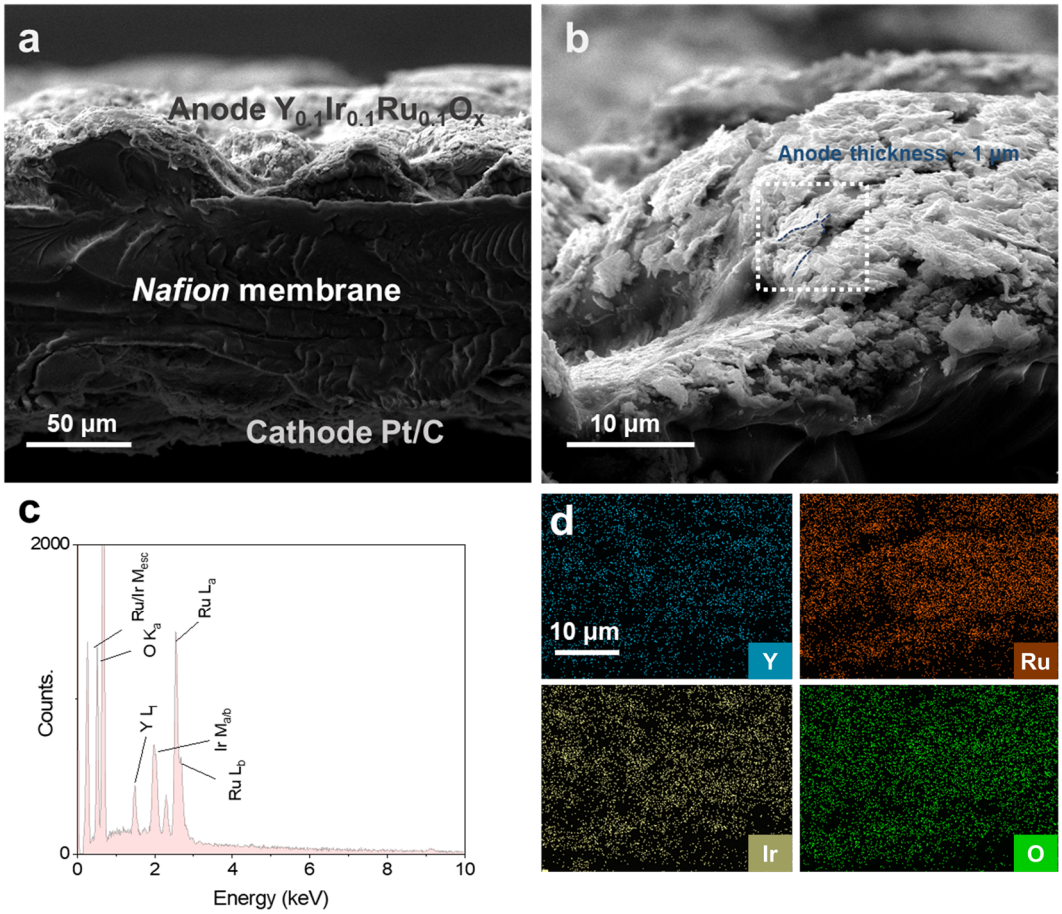

Supplementary Figure 59. (a) Cross-sectional SEM image and (b) enlarged view of the anode layer of the entire MEA after 2800 h of operation at 3 A cm^{-2}. (c) EDS data obtained by SEM-EDS. (d) SEM-EDS mappings of Y, Ir, Ru, and O elements.

(ii) XPS

The data used to characterize the metal valence states after PEMWE testing have now been replaced with XPS results of the MEA anode catalyst after 2,800 h @ 3 A cm^{-2} of stability testing. The Y 3d signal is not distinguishable due to its low loading and interference from $SiO_2 \cdot H_2O$ from gasket detachment and $-(CF_2)_n-$ species from Nafion membrane. The Ir 4f peak shows a slight shift toward the +4-oxidation state, whereas no oxidation state higher than +4 is observed for the Ru 3d region in the reacted $Y_{0.1}Ir_{0.2}Ru_{0.7}O_x$. Overall, the XPS results after long-term PEMWE operation indicate that the active-metal (Ru/Ir) oxidations of $Y_{0.1}Ir_{0.2}Ru_{0.7}O_x$ do not exhibit features associated with dissolution-prone high-valence species.

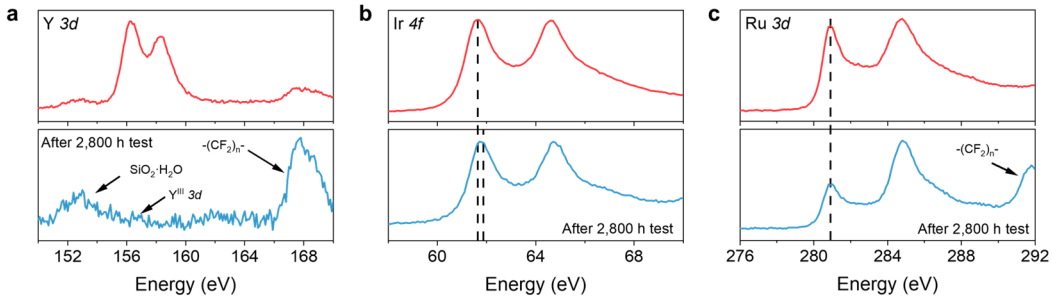

Supplementary Figure 58. XPS spectra for (a) Y *3d*, (b) Ir *4f* and (c) Ru *3d* of MEA loaded $Y_{0.1}Ir_{0.2}Ru_{0.7}O_x$ before and after 2800 h test @ 3 A cm^{-2}.

These results have been reorganized and incorporated into the revised Supplementary Information (**Supplementary Figure 58** for XPS and **Supplementary Figure 59** for SEM&SEM-EDS). For the samples after long-term PEMWE testing, we have also provided TEM and ICP-MS data in our responses to Reviewer #3, Comment 6 and Reviewer #4, Comment 6 for reference (**Supplementary Figure 60** for TEM&TEM-EDS and **Table 8** for ICP-MS)

Comment 6:

It may be informative to further explore the reaction kinetics through extended electrochemical impedance spectroscopy measurements over a wider potential range (e.g.,1.3-1.6 V vs. RHE). Fitting the data with an appropriate equivalent circuit could, if feasible, help identify features related to intermediate adsorption and desorption processes. Such exploratory analysis might provide additional insight into the kinetic characteristics of the O-O coupling step on the $Y_{0.1}Ir_{0.2}Ru_{0.7}O_x$ catalyst.

Response: We thank the Reviewer for this insightful comment. As suggested, we have appropriately adjusted the EIS measurement window to the range of 1.35-1.45 V *vs.* RHE. In addition, we have supplemented the EIS data for $Y_{0.1}Ir_{0.2}Ru_{0.7}O_x$ and $Ir_{0.2}Ru_{0.8}O_x$ for improving the ability of the EIS analysis to further describe the OER process. Under conditions where the ohmic resistance (R_u) differences among catalysts are minimized, the added data shows that $Y_{0.1}Ir_{0.2}Ru_{0.7}O_x$ consistently exhibits a smaller semicircle radius as the potential increases. At 1.45 V *vs.* RHE, fitting the EIS data for both samples reveals good agreement with the R_u- (CPE ∥ R_p) equivalent-circuit model. Focusing on the interfacial polarization resistance (R_p) in this model provides an indirect reflection of the catalyst state. Under these conditions, the fitted Rp for $Y_{0.1}Ir_{0.2}Ru_{0.7}O_x$ is 23.89 ± 0.42 Ω, whereas that for $Ir_{0.2}Ru_{0.8}O_x$ is 51.70 ± 0.54 Ω. These results further support that $Y_{0.1}Ir_{0.2}Ru_{0.7}O_x$ exhibits superior "kinetic fluidity" during

operation, i.e., a more favourable reaction pathway than $Ir_{0.2}Ru_{0.8}O_x$. These results and discussion have been incorporated into the revised manuscript (**Page 10 Line 24; Supplementary Figure 46**).

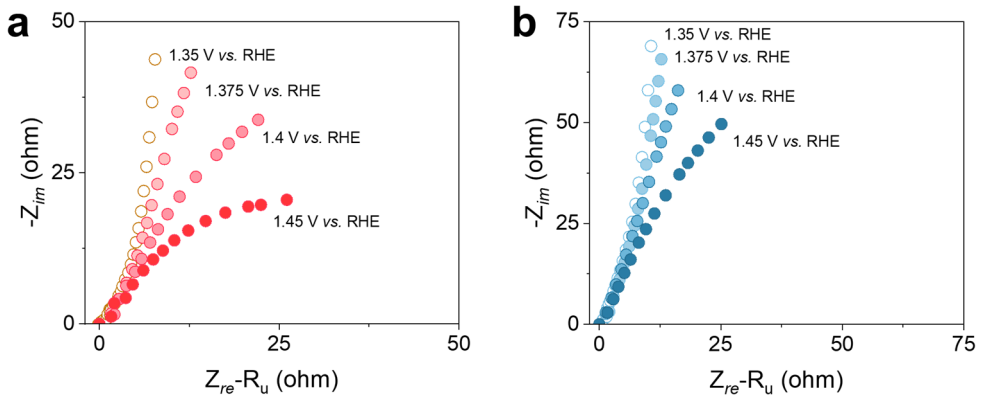

Supplementary Figure 46. Nyquist diagrams from (a) $Y_{0.1}Ir_{0.2}Ru_{0.7}O_x$ and (b) $Ir_{0.2}Ru_{0.8}O_x$.

Reviewer#3

The manuscript entitled "Directing acidic oxygen evolution catalysts toward a universal dual-site pathway" reports the design of $Y_{0.1}Ir_{0.2}Ru_{0.7}O_x$ catalysts that enable an oxide path mechanism (OPM) for acidic oxygen evolution. Through lattice-distance modulation, structural disorder engineering, and operando spectroscopy, the authors claim to achieve pervasive dual-site activation. The topic is highly relevant to the electrocatalysis and hydrogen energy communities, and the study combines advanced experimental and theoretical approaches.

We sincerely thank the Reviewer for his/her recognition and valuable feedback. In response to the Reviewer's suggestions, we have carefully revised the manuscript and prepared detailed, point-by-point responses addressing each comment. All modifications have been clearly marked in yellow in the revised manuscript and Supplementary Information.

Comment 1:

However, the novelty of the material is compromised by other Ir- and Ru-based systems in which OPM-type properties have already been demonstrated. More specifically, in a recent and very similar work by the same authors (DOI: 10.1002/adfm.202515512), which is not cited in the present manuscript, a Ru_2IrO_x-based catalyst exhibiting OPM characteristics and comparable performance (~3 A cm^{-2} at around 1.8 V) was reported. Nevertheless, the 3 A cm^{-2} @ 2800 h achieved here, with loadings of 0.4 mg_{cat} cm^{-2} for the anode and 0.5 mg_{cat} cm^{-2} for the cathode in a PEM configuration, is indeed quite impressive. The latter aspect is probably relevant enough to deserve the opportunity for revision; however, my major corrections and comments should be carefully addressed.

Response: We thank the Reviewer for reading of our work and for noting our previous work (DOI: 10.1002/adfm.202515512). Although both studies involve Ru/Ir-based catalysts for PEMWE anodes, they differ substantially in their scientific focus, catalyst design, performance, and mechanistic conclusions.

(i) Catalyst composition and structure

The catalyst developed in this work manuscript is a ternary Y-Ir-Ru oxide ($Y_{0.1}Ir_{0.2}Ru_{0.7}O_x$), whereas the previous work focused on Ru_2IrO_x-WSs. The Y elements plays a pivotal role in reshaping the electronic structure, stabilizing lattice oxygen, and modulating the reaction pathway toward the **oxide path mechanism** (**OPM**), leading to a mechanistically distinct behaviour that cannot be derived from $RuIrO_x$-WSs.

Consequently, the present system exhibits mechanistically distinct behaviour that cannot be extrapolated from $RuIrO_x$-WSs.

(ii) Mechanistic pathway assignment

The mechanistic fingerprints of $Y_{0.1}Ir_{0.2}Ru_{0.7}O_x$ are fundamentally different from those of the $RuIrO_x$-WSs. In the previous work, the key experimental signature was the dual-end *OOH adsorption, which was attributed to a neighbouring-site-accelerated deprotonation mechanism (NADM). In contrast, the present study establishes $Y_{0.1}Ir_{0.2}Ru_{0.7}O_x$ as a universal OPM catalyst with suppressed *OOH accumulation, a conclusion directly supported by DEMS detection and spectroscopic analysis.

(iii) Performance domain and objective

The present work focuses on mechanism steering that "how to design catalysts that selectively stabilizes the OPM pathway in PEMWE". This mechanistic tunability enabled by Y incorporation is the central novelty of the present study. The present catalyst delivers 3 A cm^{-2} for 2800 h at industrially relevant loadings (0.4/0.5 mg_{cat} cm^{-2}), which is substantially different in both durability and MEA configuration from our previous report (1 $mg_{cat.}$ cm^{-2} 1200 h@1 A cm^{-2}).

We have now cited the earlier work as ref. 26 in the revised manuscript and clarified these differences to avoid any misunderstanding.

Comment 2:

The authors mention that "A two-step ion etching process during XPS revealed an ~10% increase in the relative content of Y, indicating that Y is more enriched in the inner layers of the structure." However, the etching procedure itself is not described, which raises concerns regarding transparency and reproducibility. Moreover, this omission casts doubt on the chemical stability of the material. Was all the characterization and activity testing performed on the etched material? Did the authors study the material without the etching process?

Response: We thank the Reviewer for his/her insightful comments. Firstly, we would like to clarify that all other characterizations and electrochemical measurements were conducted on the $Y_{0.1}Ir_{0.2}Ru_{0.7}O_x$ sample without ion etching, which has been clarified in the revised manuscript (revised **Method-Characterization, Page 18, Line 10**).The Ar plasma etching step in the XPS experiments was performed solely for physical characterization to investigate the spatial distribution of Y within the particles and determine whether Y is uniformly throughout the nanoparticles or predominantly

concentrated in their interior.

Under Ar^+ plasma bombardment, the internal structure of the nanoparticles is randomly exposed. As XPS is highly surface-sensitive and primarily probes elemental composition within the top few nanometres, sputter-assisted XPS is commonly employed for qualitative assessment of elemental distribution between the surface and subsurface regions.

The sputtering process was performed with Ar plasma during the XPS measurements. This sputtering process was intended to randomly expose internal structural features at different depths. By comparing the measured Y *3d* signals before and after sputtering, we obtained information on the rough distribution of Y within $Y_{0.1}Ir_{0.2}Ru_{0.7}O_x$. However, due to the small particle size, where sputtering may non-uniformly expose interior domains, this approach is generally not suitable for quantitative depth profiling.

Comment 3:

The BET surface area and pore size distribution (Fig. S25) are only reported for one sample; the effect of Y incorporation on porosity compared to $Ir_{0.2}Ru_{0.8}O_x$ is not shown.

Response: According to the Reviewer's comments, we have supplemented the manuscript with the BET data of $Ir_{0.2}Ru_{0.8}O_x$, including the adsorption-desorption isotherms and the BJH pore-size distribution analysis. The supplementary data show that $Ir_{0.2}Ru_{0.8}O_x$ has a slightly lower mass-specific surface area than $Y_{0.1}Ir_{0.2}Ru_{0.7}O_x$ (46.59 *vs.* 72.04 $m^2\ g^{-1}$), which is consistent with the conclusion drawn from the double-layer capacitance analysis (Supplementary Figure 42). In terms of pore-size distribution, $Ir_{0.2}Ru_{0.8}O_x$ exhibits a slightly larger average pore size, while the overall distribution pattern remains highly similar to that of $Y_{0.1}Ir_{0.2}Ru_{0.7}O_x$. This behaviour is likely attributable to the similar synthesis routes of the two samples, combined with the higher crystallinity and larger particle size of $Ir_{0.2}Ru_{0.8}O_x$. In the initial manuscript, the y-axis of the pore-size distribution plot was incorrectly labelled ($cm^3\ g^{-1}$ instead of $cm^3\ g^{-1}\ nm^{-1}$), which has been corrected in the revised version. All of these data have now been incorporated into the revised manuscript (**Supplementary Figure 25**).

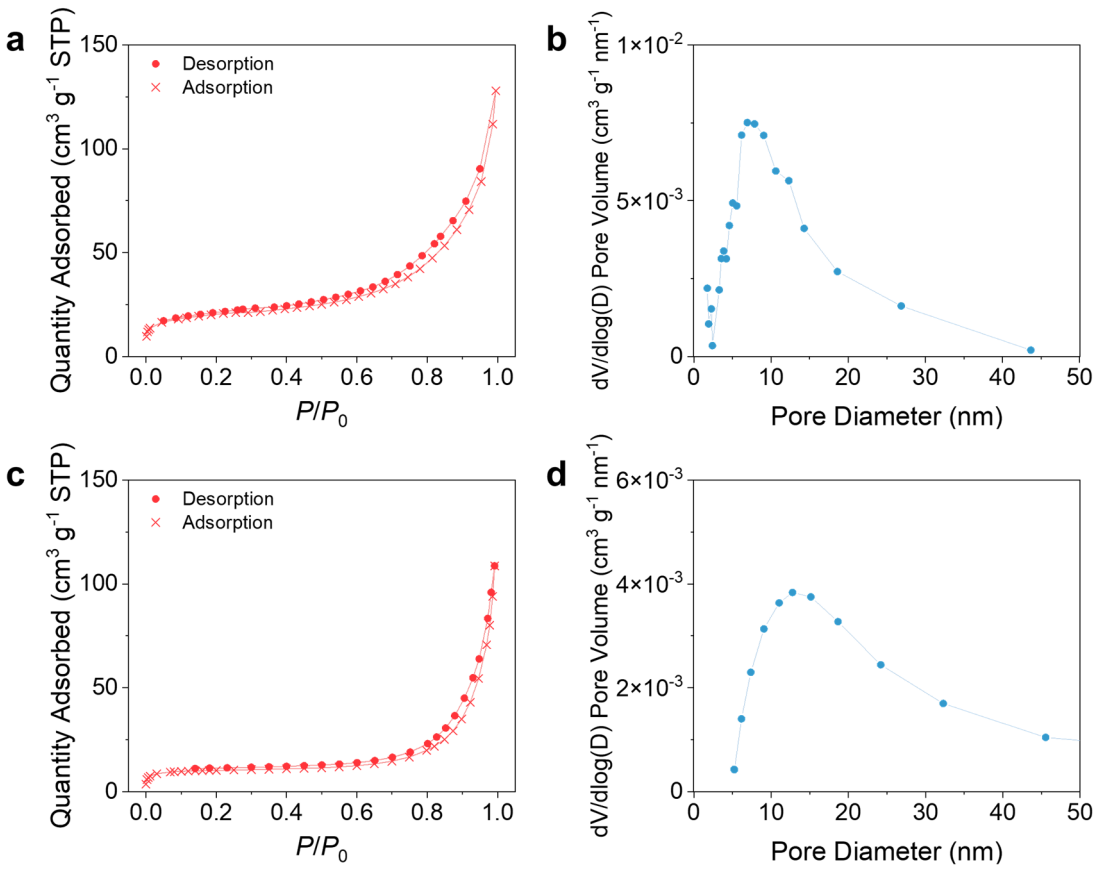

Supplementary Figure 25. (a) BET theory adsorption-desorption isotherms, and (b) corresponding Barrett-Joyner-Halenda method pore size distribution of $Y_{0.1}Ir_{0.2}Ru_{0.7}O_x$ and (c) BET theory adsorption-desorption isotherms, and (d) corresponding Barrett-Joyner-Halenda method pore size distribution of $Ir_{0.2}Ru_{0.8}O_x$.

Comment 4:

The claim that Y induces charge redistribution ("Y promotes Ir to act as a negative charge centre") is derived solely from Bader analysis and lacks experimental validation. Shifts in the XANES edge position would provide direct evidence and should be included.

Response: We thank the Reviewer for the careful consideration. We fully agree that, in most cases, Bader charge analysis is used as a complementary, averaged descriptor of the spatial preference of electronic charge distribution to support the reliability of experimentally derived valence-state changes.

The changes in the electronic properties of $Y_{0.1}Ir_{0.2}Ru_{0.7}O_x$ induced by Y incorporation have been discussed in direct connection with the XAFS results (Fig. 2 h-j). Specifically, in the initial submission, the Ir L_{III}-edge and Ru K-edge XAFS spectra, together with the corresponding valence-state analyses (Supplementary Figs. 34-38)

have provided and discussed as experimental evidence supporting these conclusions. The consistent conclusions can be drawn from the spectroscopic evidence from XPS and XANES. Specifically, the average oxidation state of Ir in $Y_{0.1}Ir_{0.2}Ru_{0.7}O_x$ (+3.0) is lower than that in $Ir_{0.2}Ru_{0.8}O_x$ (+3.7), while Ru in $Y_{0.1}Ir_{0.2}Ru_{0.7}O_x$ exhibits a higher oxidation state (+3.6) compared with that in $Ir_{0.2}Ru_{0.8}O_x$ (+3.0). This trend aligns well with the Bader charge analysis of the structural models, indicating an increase in the positive charge on Ru upon Y incorporation. We recognized that the original presentation, introducing the XANES-derived valence information first and subsequently referring back to the Bader charge analysis, suffered from a certain logical discontinuity. To enhance clarity and avoid potential confusion, and in response to the reviewer's suggestion, we have thoroughly revised this section of writing. To avoid this potential misunderstanding by readers, we have appropriately adjusted the wording in the corrected main text of the manuscript **(Page 8, Line 19).**

Comment 5:

The Tafel slope and overpotential are claimed to be "intrinsic," but uncompensated resistance (iR) correction details are lacking. EIS Nyquist plots (not just Bode) should be shown to confirm the high-frequency resistance values used.

Response: We thank the Reviewer for his/her kind reminder. In the revised manuscript, we have added the Nyquist plots used for iR-compensation calibration to **Supplementary Figure 40**. The x-axis intercept of the impedance measured at 1.5 V *vs.* RHE with an AC amplitude of 5 mV was used as the resistance value for LSV iR compensation. As shown, the uncompensated resistance during all LSV measurements falls in the range of ~50-60 Ω. Using this resistance for compensation is consistent with the prevailing practice in recent OER LSV measurements performed with rotating disk electrodes (*Joule*, 2024, 8, 450; *Adv. Mat.*, 2024, 36, 2408045.)

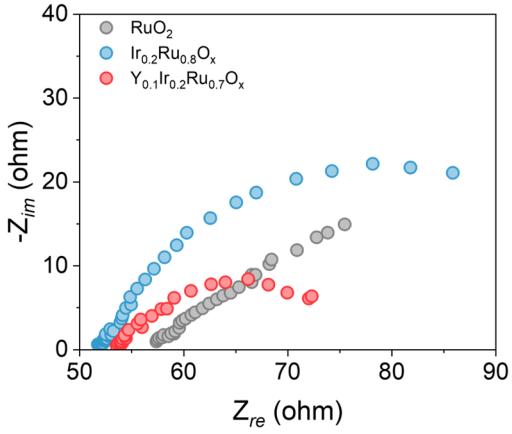

Supplementary Figure 40. Nyquist images used for iR compensation fitting. The impedance was recorded at 1.5 V *vs.* RHE, over the frequency range of 10 to 0.001 kHz with an AC amplitude of 5 mV.

Comment 6:

The durability test claims (2800 h @ 3 A cm^{-2}) are extremely strong; however, no post-mortem structural analysis (TEM/XPS/EXAFS) after this test is shown in the main text, only after 100 h (Fig. S44). This raises questions about possible microstructural evolution or Y leaching over thousands of hours.

Response: We thank the Reviewer for his/her constructive comments.

(i) TEM

The TEM images of the $Y_{0.1}Ir_{0.2}Ru_{0.7}O_x$catalyst layer after 2800 h of testing have been added to the revised Supplementary Information (**Supplementary Figure 60**). $Y_{0.1}Ir_{0.2}Ru_{0.7}O_x$ still exhibits a thin lamellar structure composed of interconnected small particles. Although the particle boundaries appear slightly blurred at higher magnification due to residual Nafion, the average particle size, morphological integrity, and the TEM-EDS results collectively indicate that $Y_{0.1}Ir_{0.2}Ru_{0.7}O_x$ remains consistent with its pre-reaction state. Moreover, its particle size (~3.53 nm) remains comparable to that before reaction, further confirming that $Y_{0.1}Ir_{0.2}Ru_{0.7}O_x$ retains its morphological integrity after the stability tests.

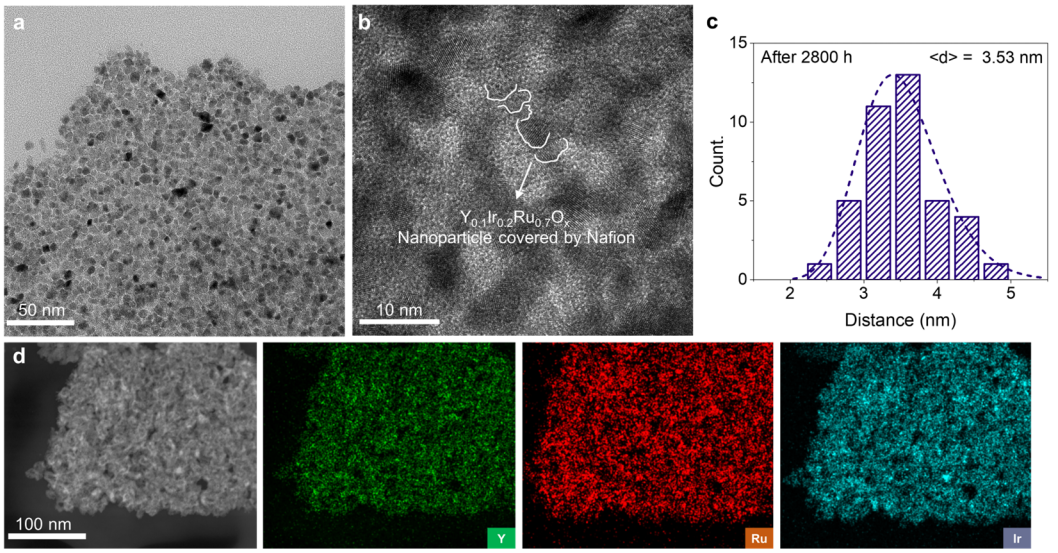

Supplementary Figure 60. Characterization of $Y_{0.1}Ir_{0.2}Ru_{0.7}O_x$ on the MEA after 2800 h of operation. (a) Single-layer $Y_{0.1}Ir_{0.2}Ru_{0.7}O_x$ after reaction. (b) Enlarged view of locally interconnected particles. (c) Particle-size distribution of $Y_{0.1}Ir_{0.2}Ru_{0.7}O_x$after reaction. (d) EDS mapping and elemental distribution.

(ii) XPS

The detailed XPS analysis of the post-test $Y_{0.1}Ir_{0.2}Ru_{0.7}O_x$ have also been discussed in our response to Comment 5 from Reviewer #2. Briefly:

1. The Y *3d* signal becomes indistinguishable due to spectral attenuation by surface-accumulated Si-O and -CF_2- species from the membrane. The presence of Y after 2800 h @ 3 A cm^{-2} is confirmed by EDS mapping and ICP-MS of the catalyst layer.

2.The Ru *3d* region shows no signature of higher oxidation states or surface RuO_x formation.

3. The Ir *4f* peak exhibits a slight shift toward Ir^{4+} from Ir^{3+} + Ir^{4+}, consistent with Ir acting as a negatively polarized site during operation. Importantly, no Ir^{6+} or other highly oxidized species are detected, indicating the absence of severe corrosion.

(iii) XAFS

Since high-precision XAFS measurements, required to determine parameters such as bond lengths, demand a significantly higher catalyst area loading density (>100 mg cm^{-2}). For the current technological limitations, reliable post-mortem XAFS measurements are unable to be performed.

In addition to TEM and XPS, we have added SEM-EDS mapping of the anode catalyst layer and its cross-section, as well as ICP-MS quantification of the retained Y content. The above-mentioned results indicate that the catalyst preserves its

morphology and composition after the 2800 h test. The above content and discussion have been incorporated into the revised manuscript. (**Supplementary Figure 58 for XPS, Supplementary Figure 59 for SEM, Supplementary Figure 60 for TEM and Table 8 for ICP-MS**).

Comment 7:

The ECSA normalization (Figs. S40-S41) is based on double-layer capacitance, which may not accurately reflect the number of active sites in disordered oxides. The authors should estimate ECSA by alternative methods such as Ru redox charge integration or underpotential deposition.

Response: We greatly appreciate these helpful suggestions from the Reviewer. In response, we have supplemented several additional methods (H-underpotential deposition, Cu-underpotential deposition, Ru redox and CO-stripping) to evaluate the ECSA. However, owing to the intrinsic physicochemical properties of RuO_2-based metal oxides, **these alternative approaches may not yield ECSA values that are more reliable than those obtained from the double-layer capacitance method.** Below, we provide a point-by-point explanation of the results from these complementary measurements.

(i) H-underpotential deposition (H_{upd})

6 μL of a catalyst ink (loading of 0.4 mg cm^{-2}) was drop-casted onto a glassy carbon rotating disk electrode (RDE, geometric area = 0.0706 cm^2). After drying under an Ar atmosphere for 30 min, cyclic voltammetry (CV) was performed in the potential window of 0.05-1.05 V *vs.* RHE at a scan rate of 50 mV s^{-1} (*Appl. Catal. B Environ.*, **2025**, 125627.). The 3rd CV cycle, where the forward and reverse scans overlapped, was selected as the representative data.

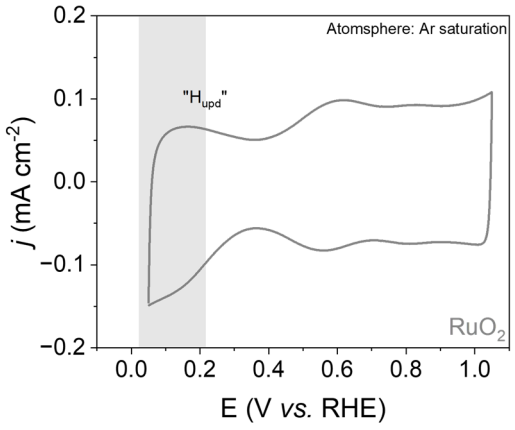

Figure R2. The j-E curves of Rutile-RuO_2 (Scan Rate: 50 mV s^{-1}) in an Ar atmosphere.

We note that, due to the competitive adsorption of oxygen-containing species, the H_{upd} measurements for oxidized Ru sites may provide limited reliability as a reference (*J. Am. Chem. Soc.*, 2013, 135, 8016). Consequently, neither the hydrogen adsorption/desorption charge nor the charge required for hydrogen adsorption/desorption per unit Ru surface area defined by Equation (*Int. J. Electrochem.* Sci., 2016, 11, 4442) can be accurately determined from the H_{upd} method. Therefore, this approach is unsuitable for ECSA quantification in our system.

(ii) Cu-underpotential deposition (Cu_{upd})

In the Cu_{upd} measurements, the RDE type, catalyst loading, and CV scan rate were kept consistent with those used in the above H_{upd} experiments. Following an initial CV scan in the base electrolyte, a mixed solution of 5 M $CuSO_4$ in 0.1 M $HClO_4$ was added to adjust the Cu^{2+} concentration to 0.05 M. Subsequent CV scans were recorded, and the first-cycle CV data after Cu^{2+} addition were compared with the pre-addition CV to assess any changes in peak features However, Cu^{2+} exhibits negligible adsorption on the RuO_2 surface (the two curves exhibit an extremely high degree of overlap); therefore, the Cu_{upd} method is not applicable to RuO_2.

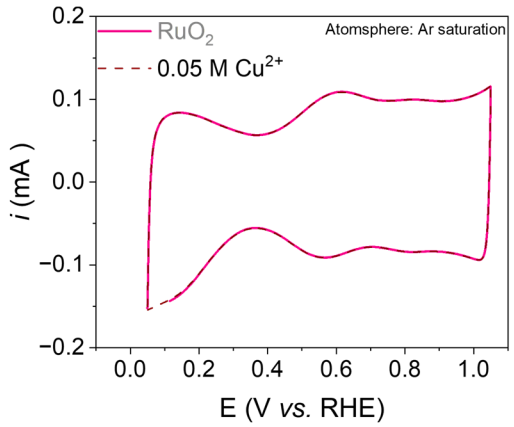

Figure R3. The j-E curves of Com-RuO_2 (Scan Rate: 50 mV s^{-1}) in an Ar atmosphere. Electrolyte: 0.1 M $HClO_4$ or 0.1 M $HClO_4$ + 0.05 M $CuSO_4$.

(iii) Ru redox

CV curves of RuO_2, $Ir_{0.2}Ru_{0.8}O_x$, and $Y_{0.1}Ir_{0.2}Ru_{0.7}O_x$ were measured between 0.2-1.45 V *vs.* RHE at a scan rate of 100 mV s^{-1}. After stabilizing the curves, the redox peaks are assigned to Ru^{3+}/Ru^{4+}, Ru^{4+}/Ru^{6+}, and Ru^{6+}/Ru^{8+} as shown in Figure R4. Among them, the most representative Ru^{3+}/Ru^{4+} peak is selected for the specific surface area determination (*Chem*, 2017, 2.5 668, *Int. J. Electrochem.,* 2018, 2018, Article ID

1273768). All subsequent calculations are based on the assumption that the dominant surface the surface facet corresponds to the RuO_2(110) crystal plane.

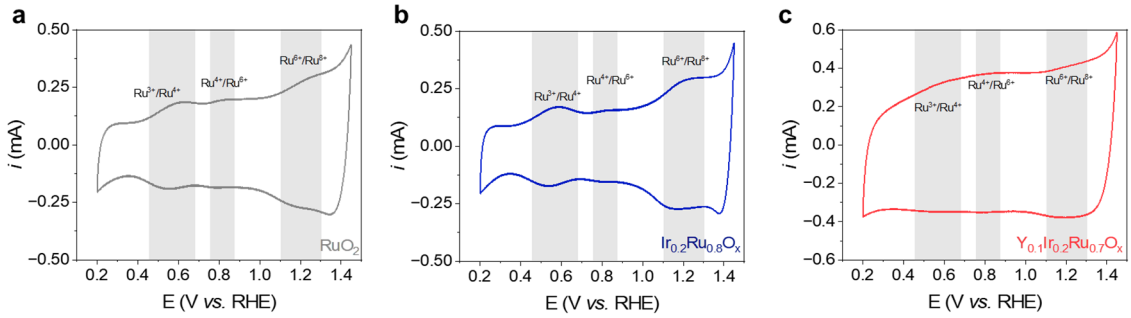

Figure. R4 Redox peaks of (a) RuO_2, (b) $Ir_{0.2}Ru_{0.8}O_x$, and (c) $Y_{0.1}Ir_{0.2}Ru_{0.7}O_x$ obtained from CV measurements.

The ECSA values are calculated from the Ru redox peak areas using the following method:

$$ECSA_{Ru_{Redox}} = \frac{Q_{Ru^{3+}/Ru^{4+}}}{N_{site\ density} \times e^-}$$

However, the ECSA values derived from the Ru redox method still suffer from notable limitations, yielding results significantly lower than those obtained via the C_{dl} method. For rutile-type nanoscale RuO_2 or $Ir_{0.2}Ru_{0.8}O_x$ the (110) facet constitutes only a fraction of the total exposed surface, yet the calculation assumes it dominates the electroactive area. Moreover, this approach neglects surface area contributions from structural defects, such as dislocations and stacking faults, that enhance the true electrochemically active surface. Consequently, for highly disordered samples like $Y_{0.1}Ir_{0.2}Ru_{0.7}O_x$ the redox peaks exhibit broader half-widths and reduced intensities, leading to an artificially suppressed ECSA (*Nat. Comm.,* 2025, 16, 1). This underestimation clearly contradicts the actual physical morphology and surface complexity of the material.

(iv) CO-stripping

As shown in Figure R5, CO adsorption on RuO_2 is inherently weak and does not yield a well-defined, potential-dependent adsorption–desorption feature. This behaviour contrasts fundamentally with that observed on metallic Ru as previously reported (*Chem. Phy. Let.*, 2002, 355, 3, 301). Therefore, CO-stripping is not suitable for determining the ECSA of RuO_2-based materials. Consequently, CO-stripping voltammetry is unsuitable for determining the electrochemical surface area (ECSA) of RuO_2-based materials.

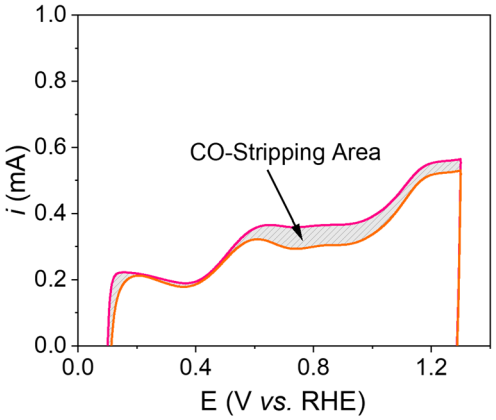

Figure. R5 Comparison of two CV cycles during the CO-stripping measurement. The shaded area represents the differential CO-stripping charge.

In summary, as presented in Table R1, all methods except the C_{dl} approach are compromised, either by variable adsorption characteristics inherent to RuO_2-based surfaces or by competitive interactions among coexisting surface species, leading to ill-defined signals or ECSA values that deviate significantly from the physically realistic range.

Table R1. ECSA from Rutile-RuO_2 obtained by different calculation methods

Calculating method	ECSA (m^2 g^{-1})
Double-layer capacitance (C_{dl})	112.29
Cu_{upd}	Invalid
CO-stripping	Invalid
H_{upd}	Invalid
Ru redox	2.25

Comment 8:

The signals in the FTIR spectra correspond to bands, not discrete peaks. The authors should provide the exact wavenumber positions of all relevant bands in the figures so that the discussion can be followed more precisely.

Response: We thank the Reviewer for his/her careful reading and kind reminder. As suggested, we have explicitly **labelled the exact wavenumber** positions of all relevant bands in Fig. 4c, d and clarified them in the figure captions.

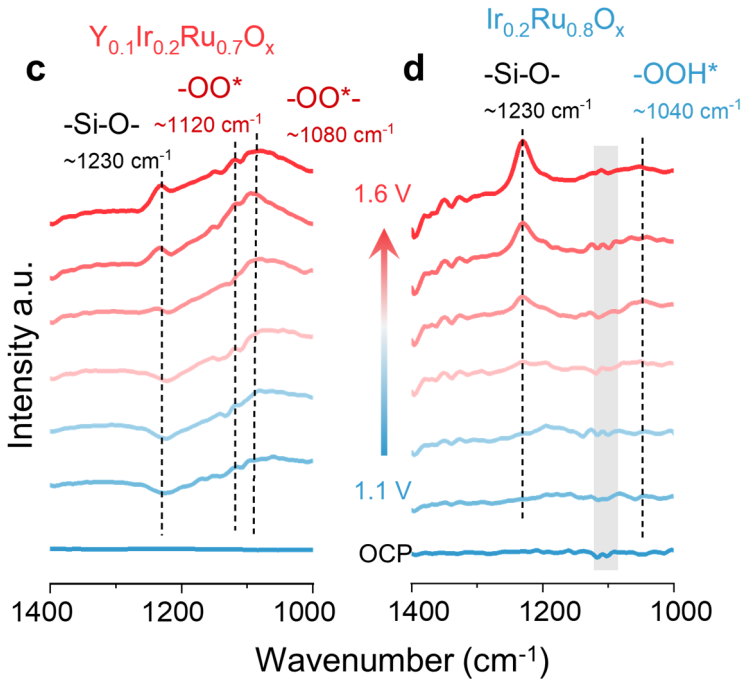

Figure. 4c-4d c, ATR-FTIR intensity-potential spectrum of $Y_{0.1}Ir_{0.2}Ru_{0.7}O_x$ and d, $Ir_{0.2}Ru_{0.8}O_x$. DEMS signal and integrated-intensity plot for ^{18}O-labelled $Y_{0.1}Ir_{0.2}Ru_{0.7}O_x$.

Comment 9:

I am highly sceptical about the interpretation of the FTIR bands. The spectra in Figures 4c and 4d show no clear or significant differences. The authors assign the band at approximately 1230 cm^{-1} to OO species; however, the cited reference (Ref. 38), which forms the basis for this assignment, actually attributes this band to Si-O-Si vibrations, while the -OO* feature is reported closer to 1200 cm^{-1}. In this region, the Y-free sample displays a higher band intensity, which could simply arise from greater Si exposure on the surface-perhaps due to a lower catalyst loading. This lower loading could also explain the weaker signal at ~1070 cm^{-1} in the Y-free sample, which the authors attribute to bridging oxygen species. Hence, more intense and clearly distinguishable FTIR features are needed before the claim of OPM promotion in the Y-containing catalyst can be considered reliable.

Response: We thank the Reviewer for the careful reading and highly insightful comments. We recognize that, in the original manuscript, ambiguous peak labelling in the figure captions and the absence of a clear one-to-one correspondence between labels and spectral features could lead readers to mistakenly assign the -OO* band (which is actually centred at 1120 cm^{-1}) to the nearby ~1230 cm^{-1} feature associated with Si-O vibrations. To address this potential misinterpretation, we have revised **the annotations**

of Fig. 4c and d in the resubmitted version.

Comment 10:

Why does the 1070 cm^{-1} band shift with potential? The manuscript should explain this potential-dependent behaviour.

Response: We thank the Reviewer for his/her insightful comments. With increasing potential, changes in the interfacial electric field and the surface coverage of oxygenated intermediates lead to a pronounced intensification and a concomitant shift of the -OO* band at ~1070 cm^{-1}. This behaviour can be attributed to the electrochemical Stark effect commonly observed in infrared spectroscopy, where vibrational frequencies respond to variations in the local electric field and dipole-field interactions. (*Molecular Spectra and molecular structure-Vol I.* Vol. 1. Read Books Ltd, 2013; *Fundamentals of Molecular Spectroscopy*, 4th ed., McGraw-Hill, 1994). In the present system, the dominance of universal OPM promotes the accumulation of intermediates such as -OO* with shifting potential, thereby providing the interfacial environment in which such Stark-type responses become observable. A corresponding explanation has been incorporated into the revised Supplementary Information (**Notes for Supplementary Figure 71**).

Comment 11:

The authors should carefully verify the consistency between the labels in Figure 4 and those mentioned in the text, as some appear mismatched.

Response: We thank the Reviewer for his/her careful attention to the details. We acknowledge that some inaccuracies were introduced during the calibration of the text related to Figure 4 in the initial submission. These issues have now been corrected and revised in the resubmitted manuscript.

Comment 12:

Regarding the DEMS experiments, the authors state that "the intensity of $^{36}O_2$ is unusually high." I fully agree; however, further clarification is needed. Was Ar used to deoxygenate the electrolyte? Ar^+ produces a signal at m/z = 36, which could artificially elevate the baseline. Did the authors perform any calibration or blank tests prior to these measurements?

Response: We greatly appreciate the Reviewer for his/her helpful suggestions. In fact,

in the presented DEMS experiments, potential interference from ambient and residual chamber gases has been carefully accounted for particularly with respect to the *m/z* = 36 signal, which is critical for identifying the evolution of $^{36}O_2$. Before the measurements, the electrolyte was thoroughly deoxygenated and the chamber was evacuated to near vacuum. During testing, apart from gases generated by the electrochemical reactions, no external gas sources were introduced into the electrolyte. It is important to clarify that argon constitutes approximately 0.93% of the Earth's atmosphere, while the natural isotopic abundance of ^{36}Ar within atmospheric Ar is only ~0.003% (*Geochim. Cosmochim. Acta*, 2006, 70, 4507). Once the analysis chamber is evacuated to a base pressure, at which the DEMS signals at *m/z* = 32, 34, and 36 stabilize (i.e., no longer drift), the residual amount of ^{36}Ar becomes negligible and is unlikely to contribute meaningfully to the observed signal. To further address the Reviewer's concern, we have included a representative segment of *m/z* = 36 background data recorded under conditions where no $^{36}O_2$ was generated.

Additionally, DEMS is a small mass spectrometry device, and in order to minimize interference from non-molecular ion sources, its ionization source operates at a relatively low energy, making it more difficult for the Ar atoms entering the chamber to be dissociated (*Acta Chimica Sinica*, 2020, 78, 504.). Therefore, DEMS has intrinsic difficulty in capturing $^{36}Ar^+$: a species with low density in air and poor ionization efficiency, which results in low interference by ^{36}Ar during the $^{36}O_2$ test of the *m/z* = 36 signal. As shown in Figure R6, when no $^{36}O_2$ is produced, the MS background noise at *m/z* = 36 remains generally ~10^{-12}, which clearly supports the point that $^{36}Ar^+$ could probably not interference MS signal.

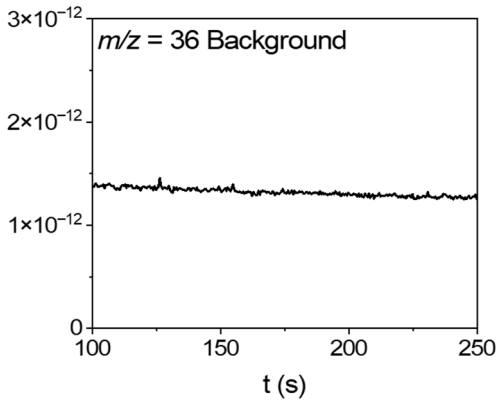

Figure. R6 DEMS background in the absence of $^{36}O_2$.

The mass spectrometry signal shown in the Figure was recorded prior to the onset of

the electrochemical test, after the chamber had been evacuated to a base pressure, meeting the experimental requirements. Details regarding the DEMS testing procedure can be found in the revised manuscript (**Page 21, Line 4**).

Comment 13:

Finally, the manuscript concludes that "almost all active sites follow the OPM pathway." The current data do not allow quantification of the fraction of OPM-active sites. To support such a strong statement, additional operando experiments—such as O K-edge XAS, Raman under bias or isotope-dependent Tafel analyses—would be necessary.

Response: We thank the Reviewer for his/her thoughtful suggestions. We agree with the Reviewer that the statement "almost all active sites follow the OPM pathway" was overly definitive. To avoid any potential misinterpretation, we have revised it to: "clearly dominant during OER on $Y_{0.1}Ir_{0.2}Ru_{0.7}O_x$" which more accurately reflects the strength and scope of the current experimental evidence. Below, we provide detailed responses regarding each characterization method.

For (i) O K-Edge XAS and (ii) Raman under bias

After careful discussion, we have decided not to add O K-edge XAS or Raman data to further supplement the manuscript. The reasons are as follows:

1. O K-edge XAS has intrinsic limitations in extracting quantitatively meaningful information from short-lived reaction intermediates. In particular, key intermediates in the OPM pathway, such as transient -O-O- species, generally exhibit low surface coverage (*Nat. Catal.,* 2020, 3, 516). In contrast, O K-edge XAS is more suitable for probing the overall distribution of oxygen states in the catalyst (*Phys. Rev. B*, 1989, 40, 5715). We therefore consider that O K-edge XAS would not play a decisive role in establishing more quantitative relationships for the reaction pathways of $Y_{0.1}Ir_{0.2}Ru_{0.7}O_x$

2. Raman spectroscopy primarily probes relatively stable surface or near-surface intermediates. However, the stretching vibrations of key OPM intermediates such as -O-O- are Raman-inactive or weakly Raman-active. Moreover, Raman laser irradiation may degrade these photo-sensitive oxygen-containing intermediates. For these reasons, in the initial submission we chose ATR-FTIRAS, which provides more comprehensive and effective information than Raman, for characterizing -OO* and related intermediates (*Molecular Vibrations*, Courier Corp., 1980; *Chem. Rev.*, 2023, 123, 12135). More importantly, neither FTIR nor Raman spectroscopy can directly establish

a quantitative relationship between absorption/scattering intensity and the actual reaction rate or pathway contribution. As such, adding these measurements would be unlikely to substantially improve the completeness or rigor of the current manuscript.

For (iii) isotope-dependent Tafel slope by D2O solution

By comparing the kinetic behaviour of the catalysts in D_2O and H_2O at different current densities (i.e., Tafel slopes; *Nat. Chem.,* 2025, 1), it is possible to semi-quantitatively evaluate whether the reaction kinetics depend on proton–electron concerted transfer steps (i.e., CPET). Following the protocol in the literature, we measured and compared the kinetics of $Y_{0.1}Ir_{0.2}Ru_{0.7}O_x$ and $Ir_{0.2}Ru_{0.8}O_x$ in protonic (H_2O) and deuterated (D_2O) environments. In all cases, the electrolyte was 0.1 M $HClO_4$ (or $DClO_4$), and the residual proton content in the deuterated electrolyte was below 2%. As shown in the updated Supplementary Figure 76, $Y_{0.1}Ir_{0.2}Ru_{0.7}O_x$ exhibits similar kinetic behaviour in H_2O and D_2O as the current density increases, whereas $Ir_{0.2}Ru_{0.8}O_x$ shows distinctly different kinetics, with significantly slower behaviour in the D_2O environment. In the AEM pathway, the rate-determining step, formation of *OOH is a typical CPET process; therefore, $Ir_{0.2}Ru_{0.8}O_x$ is expected to display a pronounced isotope effect under different protonic environments. In contrast, although DFT calculations indicate that the rate-determining step for $Y_{0.1}Ir_{0.2}Ru_{0.7}O_x$ shifts to CPET-type *OH formation (Fig. 1f), the associated energy barrier is comparable to that of the non-CPET O-O coupling step. This may account for the weak dependence of $Y_{0.1}Ir_{0.2}Ru_{0.7}O_x$ on proton transfer.

While these results do not provide a direct quantitative metric, the Tafel isotope effect nevertheless offers additional kinetic support for the conclusion that $Y_{0.1}Ir_{0.2}Ru_{0.7}O_x$ predominantly follows the OPM pathway. As described above, these discussions have been incorporated as **Supplementary Figure 77.**

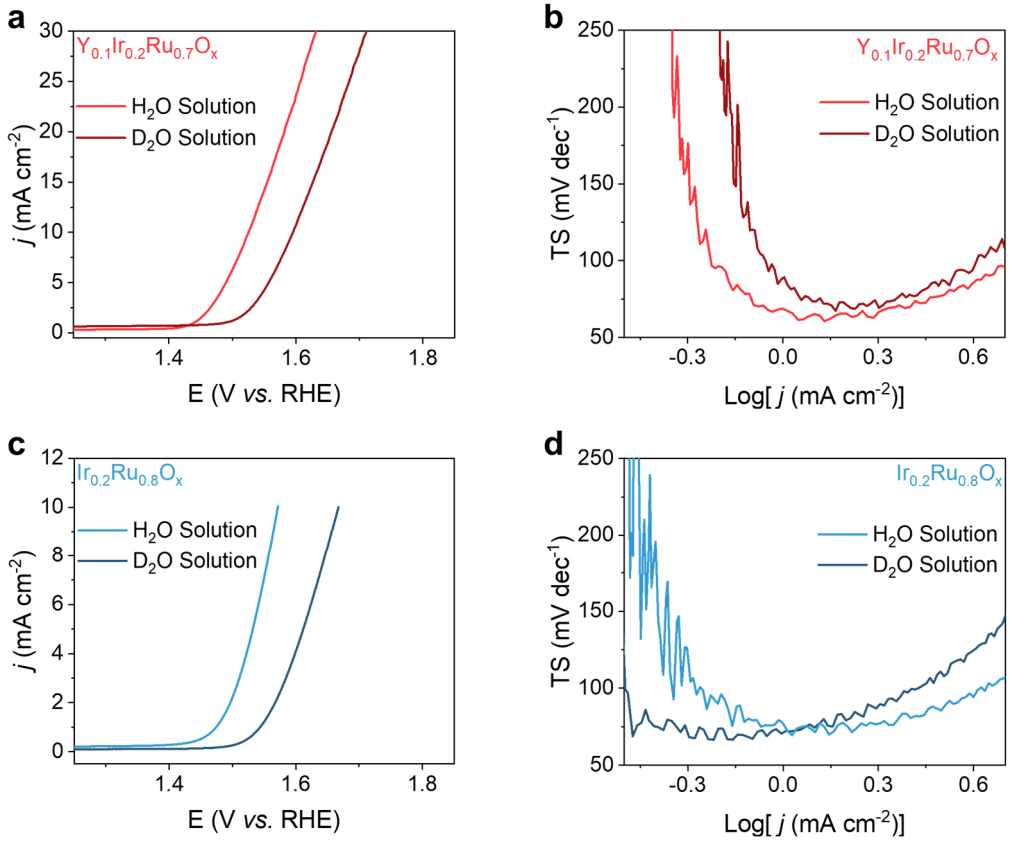

Supplementary Figure 77. (a) LSV curves of $Y_{0.1}Ir_{0.2}Ru_{0.7}O_x$ measured in H_2O and D_2O, and (b) corresponding TS-Log *j* plots. (c) LSV curves of $Ir_{0.2}Ru_{0.8}O_x$ measured in H_2O and D_2O, and (d) corresponding TS-Log *j* plots.

Note: due to the surface passivation of Nb and the slower bubble-dispersion dynamics in the absence of external hydrodynamic assistance, the LSV curves collected on Nb foil generally appear not as smooth as those on a RDE.

In summary, considering all the available operando evidence, including DEMS, ATR-FTIRAS, TafelIE, the additional RRDE measurements provided in response to Reviewer #2, Comment 4 (to verify the inactivity of the AEM key intermediate -OOH), and the TMA^+ poisoning experiments added in response to Reviewer #4, Comment 2 (to exclude LOM contributions), we acknowledge that these new results do not provide a more direct quantitative relationship than the original DEMS data. Nevertheless, after eliminating potential interfering factors through this revision, we continue to support the main conclusion that **$Y_{0.1}Ir_{0.2}Ru_{0.7}O_x$ follows a universal OPM pathway**.

Reviewer#4

The manuscript aims to develop a universal design strategy for acidic OER catalysts following the OPM. The authors report a designed composition, Y0.1Ir0.2Ru0.7Ox, which achieves 3A cm^{-2} at 1.75 V in PEM water electrolysis and remains stability for 2800 h with a degradation rate of 0.0625 mV h^{-1}. The study contains interesting results, but several substantive issues must be addressed before the manuscript can be considered for publication.

We sincerely appreciate the Reviewer's recognition and constructive comments, which have greatly helped us to improve the quality and clarity of this manuscript. We have carefully addressed all concerns and provided detailed, point-by-point responses below.

Comment 1:

Inconsistency between text and figures. There is a serious inconsistency between the text and the figures in the Reaction pathway elucidation section. Figs. 4i and 4h are referenced in the text (page 14, line 7; page 15, line 1), but they are missing from the manuscript. Please check and correct the figure numbering.

Response: We appreciate the Reviewer's careful attention to details. As suggested, the discrepancy between the text and figure references (specifically, the incorrect citation of Fig. 4h, i on Pages 14 and 15) has been identified and fully corrected in the revised manuscript. All figure labels and in-text citations have been carefully cross-checked and updated for consistency (**Page 15, Line 8**).

Comment 2:

The authors conclude that $Y_{0.1}Ir_{0.2}Ru_{0.7}O_x$ follows OPM while $Ir_{0.2}Ru_{0.8}O_x$ follows AEM. However, LOM pathways cannot be fully excluded on the basis of the current evidence. I recommend a chemical-probe test (e.g., with and without TMA) or other established isotope/probe experiments to distinguish OPM from LOM unambiguously. Also, the Raman/IR wavenumber assigned to OOH (reported here) differs from values reported in the literature (e.g., ~986 cm^{-1}, Nat. Catal., 2021, 12, 1012-1023); please reconcile or justify this discrepancy.

Response: We greatly appreciate these helpful suggestions from the Reviewer.

(i) TMA^+ poisoning to eliminate LOM.

Following the Reviewer's suggestion, and in accordance with prior studies (*Angew. Chem*., 2017, 129, 8778; *J. Am. Chem. Soc.,* 2024, 146, 33663), we have supplemented a comparison of LSV curves before and after TMA^+ poisoning. Specifically, after

recording the baseline LSV under interference-free conditions, additional LSV measurements were carried out in an electrolyte containing 0.1 M TMA^+. In this process, TMA^+ and related species are known to block peroxide-like intermediates involved in pathways such as LOM, whereas the coupled intermediates operative in the OPM pathway are not inhibited (*Adv. Mater.,* 2025, 37, 2420159). $Y_{0.1}Ir_{0.2}Ru_{0.7}O_x$ shows no performance degradation in the presence of TMA^+ with its LSV characteristics essentially unchanged (Supplementary Figure 75 in the revised Supplementary Information). In contrast, $Ir_{0.2}Ru_{0.8}O_x$ exhibits a slightly noticeable decrease in activity, indicating that the catalytic process of $Ir_{0.2}Ru_{0.8}O_x$ is partially inhibited by TMA^+. This observation is consistent with the DEMS results in Fig. 4. After ^{18}O labelling, the $^{34}O_2/^{32}O_2$ ratio of $Ir_{0.2}Ru_{0.8}O_x$ is higher than the typical natural abundance of ^{18}O in air (≈0.5%), suggesting that a minor contribution of lattice oxygen is involved (*Adv. Mat.,* 2025, 37, e11461). We agree that a minor LOM contribution cannot be entirely excluded. Indeed, both DEMS and TMA^+ poisoning indicate the presence of a small LOM fraction in $Ir_{0.2}Ru_{0.8}O_x$, whereas $Y_{0.1}Ir_{0.2}Ru_{0.7}O_x$ remains unaffected. These results confirm that LOM is not a dominant pathway for the typical catalyst. We have adjusted the corresponding description in the main text to align with this fact in the revised version **(Page 15 Line 12)**.

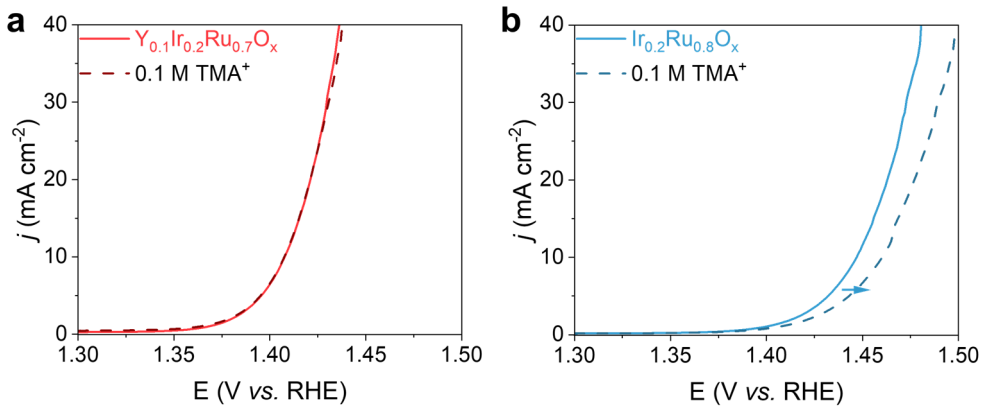

Supplementary Figure 66. Comparison of the LSV curves of (a) $Y_{0.1}Ir_{0.2}Ru_{0.7}O_x$ and (b) $Ir_{0.2}Ru_{0.8}O_x$ before and after TMA^+ poisoning.

(ii) The difference from FTIR signal labelling

The ATR-FTIR spectra were collected using a silicon prism under total-reflection conditions (Bruker Vertex 70V). It is well established that the $\nu_{(OO^*)}$ positions can shift depending on prism material, penetration depth, and evanescent-field distribution. The synchrotron-based grazing-incidence setup used in Lin et al. (*Nat. Catal.,* 2021, 12,

1012) therefore yields a different field environment. As such, a shift in absolute peak position is expected. Importantly, the evolution trend and potential-dependent behaviour of the ν(OO*) band remain consistent with OPM-type surface intermediates.

The above content and discussion have been incorporated into the revised manuscript (**Page 13, Line 21 and Supplementary Figure 66**).

Comment 3:

The DFT-guided microscopic structural design section lacks logical coherence with later sections. The synthesis, characterization and electrochemical performance of various samples (such as $Y_{0.1}Ir_{0.2}Ru_{0.7}O_x$ and $Ir_{0.2}Ru_{0.8}O_x$, et al.) are described later in the manuscript, yet their electrochemical data (e.g., $YRuIrO_x$ and $RuIrO_x$) already appear in earlier sections (Fig. 1e, Supplementary Figs. 2–4 and 7). In addition, the overpotential of YRuIrOx and $Y_{0.1}Ir_{0.2}Ru_{0.7}O_x$ differ noticeably. Are these samples identical and prepared via the same synthesis route? Please clarify the sample naming and experimental sequence to avoid confusion.

Response: We thank the Reviewer for the careful scrutiny of the logical coherence of the manuscript. In response to these comments, we have revisited and reorganized the content referred to by the Reviewer (**Fig. 1e, Supplementary Figs. 2-4 and 7**). To eliminate ambiguity, we have now standardized the sample nomenclature throughout the manuscript. All experimentally synthesized samples are denoted as $M_aIr_bRu_cO_x$ (M = Y, Sr, Sc, Mg, or none; e.g., $Ir_{0.2}Ru_{0.8}O_x$, $Sr_{0.1}Ir_{0.2}Ru_{0.7}O_x$ or $Y_{0.05}Ir_{0.2}Ru_{0.75}O_x$), whereas all computational models are consistently referred to as $MRuIrO_x$. In the main text, we have also clarified that $MRuIrO_x$ refers to the computational models, whereas $M_aIr_bRu_cO_x$ denotes the experimentally synthesized samples. We have revised the description in the main text to ensure that readers can clearly distinguish between the computational results and the experimental data in the revised manuscript (**Page 4 Line 16**).

Regarding the Reviewer's concern about inconsistencies in the reported overpotential values, we have carefully re-examined all relevant data sources. We found that, due to an oversight in the initial submission, the data in this figure that should correspond to $Y_{0.1}Ir_{0.2}Ru_{0.7}O_x$ were mistakenly replaced with those of $Y_{0.05}Ir_{0.2}Ru_{0.75}O_x$. We also clarify that, unless otherwise specified, all experimental samples were prepared using the same procedures described in the "Methods section", and that the sample originally intended and shown in Supplementary Fig. 2 is $Y_{0.1}Ir_{0.2}Ru_{0.7}O_x$. These issues

have now been corrected, and the experimental samples and computational models have been clearly distinguished by name as requested. The corrected **Supplementary Figure 2** is as follows:

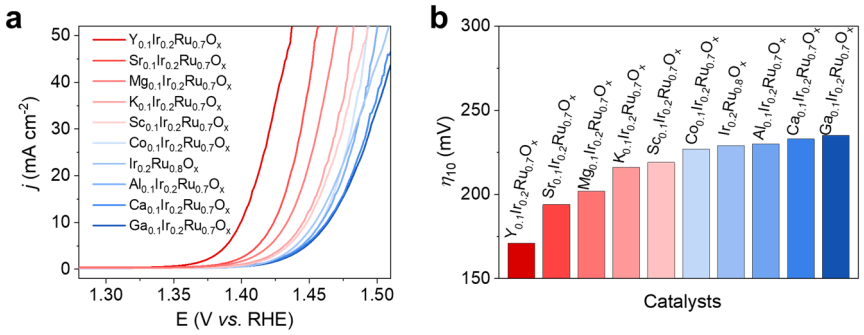

Supplementary Figure 2. (a) LSV curves and (b) overpotential at 10 mA cm^{-2} of $M_{0.1}Ir_{0.2}Ru_{0.7}O_x$ based catalysts with different metal heteroatoms.

Comment 4:

The hypothesis states that densely packed dual sites with short Ru–Ru_1 bonds favour OPM. However, Fig. 1f presents step energy barriers only for Y0.1Ir0.2Ru0.7Ox. To support the claim convincingly, perform equivalent calculations for other samples with similar Ru–Ru_1 distances (e.g., $RuIrO_x$, $SrRuIrO_x$; see Figs. 1c and 1e). Comparative DFT results will demonstrate whether the short Ru–Ru_1 distance itself is the decisive factor.

Response: We thank the Reviewer for his/her careful attention to the rigor of the DFT calculations. We have supplemented the manuscript with DFT-derived energy step diagrams for $RuIrO_x$ and $SrRuIrO_x$ models under both the AEM and OPM pathways, as shown in Supplementary Figure 19 in the revised Supplementary Information. For $RuIrO_x$ with a longer Ru-Ru_1 bond length (3.118 Å), the calculated OPM energy barrier (0.82 eV) is higher than that of AEM (0.79 eV), indicating that OPM is less favourable, which is consistent with experimental observations. In contrast, for the $SrRuIrO_x$ model, after the Ru-Ru_1 bond length is shortened (3.091 Å), the OPM barrier (0.49 eV) becomes lower than the AEM barrier (0.58 eV). This trend is consistent with our earlier conclusion in the initial submission that the $YRuIrO_x$ model, featuring a shorter Ru-Ru_1 bond length, exhibits a lower calculated energy barrier. The added information has been incorporated into the revised manuscript (**Page 6, Line 3 and Supplementary Figure 19**).

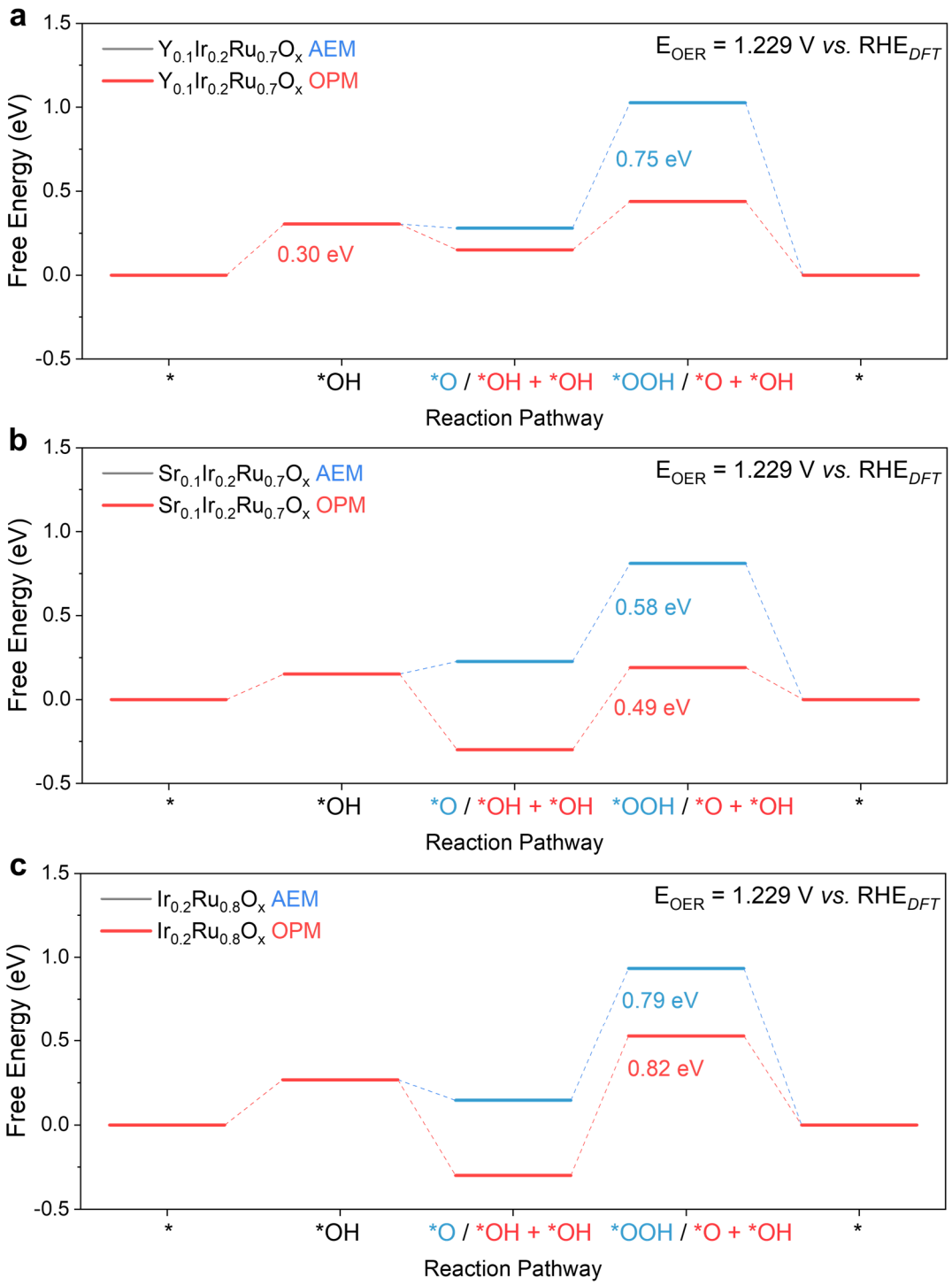

Supplementary Figure 19. Free-energy step diagram of (a) $YRuIrO_x$ (b) $SrRuIrO_x$, and (c) $RuIrO_x$ at 1.229 V *vs.* RHE *via* AEM and OPM pathways.

Comment 5:

The respective roles of Ir and Ru in facilitating OPM are not clearly declared. Specify which atomic sites were modelled as active centres in the calculations and discuss how

Ru and Ir individually contribute to the proposed OPM pathway.

Response: We thank the Reviewer for his/her attention to the site specificity. We clarify our perspective on the distinct roles of Ru and Ir from the following aspects.

(i) Specify which atomic sites were modelled as active centres in the calculations

In the DFT modelling calculations, we consistently consider the Ru-Ru sites as the active centres for the OPM reaction.

(ii) Discussing how Ru and Ir individually contribute to the proposed OPM pathway

In the manuscript, Ir plays an indirect but essential role by modulating the electronic structure and local lattice geometry of the Ru sublattice. Consistent with several recent studies (*Nat. Comm*., 2023, 14, 5365.), Ir incorporation stabilizes the Ru-Ru dual-site configuration, adjusts the local electronic environment.

(iii) Scope and intention of the DFT modelling

Our rationale for cautiously selecting Ru, rather than Ir, as the computational active site is as follows:

1. In samples that can be regarded as mixed oxides, the variations in the electronic properties of Ru and Ir are intrinsically coupled. As shown in Fig. 3 of the main text, our XAFS observations reveal consistent trends in the Ru/Ir valence-state changes between $Y_{0.1}Ir_{0.2}Ru_{0.8}O_x$ and $Ir_{0.2}Ru_{0.8}O_x$ (*Advanced Inorganic Chemistry*, 2nd ed., Interscience, 1966). Separately discussing the intrinsic differences between Ru and Ir would therefore bias the interpretation and undermine the significance of the DFT calculations.

2. Ru and Ir themselves exhibit only minor differences in intrinsic electronic properties, possessing similar electronic structures and ionic radii (*Chemistry of the Elements*, 2nd ed., Butterworth-Heinemann, 1997). In DFT studies aimed at elucidating reaction pathways such as OPM, artificially distinguishing Ru and Ir active sites would, in fact, render the conclusions less reliable.

For the above reasons, we intentionally do not differentiate between Ru and Ir sites in the DFT calculations and instead treat Ru as the representative active site. Based on the Reviewer's comment, and to avoid any potential misinterpretation or misjudgement of the DFT models by readers, we have revised the DFT-related description in the Methods section of the revised manuscript **(Page 22, Line 27).**

Comment 6:

Potential dissolution of Y and related surface evolution in acid appear overlooked. Does

$Y_{0.1}Ir_{0.2}Ru_{0.7}O_x$ retain the nominal atomic ratio after OER test? Characterizations should be employed before and after stability test, such as ICP-MS, SEM, TEM and EDS.

Response: We thank the Reviewer for his/her meaningful comments. As suggested, we have supplemented the characterization of $Y_{0.1}Ir_{0.2}Ru_{0.7}O_x$ on the MEA after 2800 h of stability testing using multiple techniques, including ICP-MS, SEM, TEM, and EDS. The improved characterization results are presented below.

(i) ICP-MS measurement

A ~0.1 cm^2 section of the MEA after the 3 A cm^{-2} stability test was cut out and subjected to acidification following super-microwave digestion, and diluted to 25 mL × 3 parts. The residual metal content in the MEA fragment was then measured by ICP-MS (Agilent 7800).

Table 8. ICP-MS results from diluted MEA. (unit: ppb)

Elements	1st sample	2nd sample	3rd sample	Average
Y	7.575	7.528	6.678	7.260
Ir	48.313	50.118	49.389	49.273
Ru	236.029	244.964	243.968	241.654

When converted to molar amounts, the measured mass ratio after testing is approximately Y: Ir: Ru = 1:6.79:33.3. Combined with the higher oxidation state of Ir in $Y_{0.1}Ir_{0.2}Ru_{0.7}O_x$ and the ICP-MS analysis of the electrolyte (Fig. 3e and Table 5), it is evident that Y exhibit a tendency to leach during the stability test. This is also consistent with the conclusion that etching XPS (Fig. 2g), indicating that Y is more easily dissolved. These discussion has been incorporated into the revised manuscript (**Table 8 and Page 13, Line 8**).

(ii) Measurements of SEM, SEM-EDS, TEM, and TEM-EDS

We have supplemented the manuscript with SEM images of the MEA cross-section after the 2800 h durability test (Fig. 3f), as well as HR-TEM images of the post-reaction $Y_{0.1}Ir_{0.2}Ru_{0.7}O_x$ in the anode catalyst layer (Supplementary Figure 60). The corresponding EDS spectra of these samples have also been included. The SEM results can be found in the response to Reviewer #2, Comment 5, and the HR-TEM images are provided in the response to Reviewer #3, Comment 6. Overall, $Y_{0.1}Ir_{0.2}Ru_{0.7}O_x$ maintains its original lamellar morphology even after prolonged high-current-density operation, showing no signs of dissolution such as blurred boundaries or particle aggregation. As described above, these discussions have been incorporated into the

revised manuscript **(Supplementary Figure 59 for SEM and 60 for TEM)**.

(iii) XPS measurement

XPS spectra of the anode surface of the MEA after durability testing have been provided (Reviewer #2, Comment 5). In summary, apart from the Y *3d* signal, which is not clearly visible due to its low amount and interference from surface species (-CF_2- or hydrated SiO_2 from gasket detachment), the Ru *3d* and Ir *4f* XPS spectra indicate that both elements retain stable valence states after the 2800 h test. No signatures of dissolved species such as Ru^{6+}/Ir or Ru^{8+} are observed. As described above, these discussions have been incorporated into the revised manuscript **(Supplementary Figure 58)**.

Comment 7:

The statements "exceptional operational stability (>2,800 h @ 3 A cm^{-2})" (Abstract) and "exceptional stability for 2,800 h" (p. 12) are overstated given the reported potential degradation (≈ 175 mV). Remove the word "exceptional" or temper the language and explicitly report the absolute potential increase (175 mV) and the degradation rate (0.0625 mV h^{-1}) so readers can judge practical relevance.

Response: We sincerely thank the Reviewer for his/her careful and repeated scrutiny of the wording throughout the manuscript. Based on these suggestions, we have reviewed the restraint and appropriateness of descriptive wording in the main text and have specifically refined the descriptions related to stability. These semantic changes have been revised in the resubmitted manuscript **(Page 1, Line 22; Page 3, Line 20; Page 13, Line 6)**.

i.e.,

…with ~~exceptional~~ operational stability (> 2,800 h@3 A cm^{-2}) in proton exchange membrane water electrolysis, with 0.0625 mV h^{-1} decay rate.

…with $Y_{0.1}Ir_{0.2}Ru_{0.7}O_x$ anode demonstrates ~~exceptional~~ improved performance, delivering a low cell voltage of 1.75 V at a high current density of 3 A cm^{-2} with ~~remarkably~~ low catalyst loadings (0.1 mg_{Ir} cm^{-2} and 0.3 mg_{Ru} cm^{-2}).

…$Y_{0.1}Ir_{0.2}Ru_{0.7}O_x$ maintains ~~exceptional~~ stability for 2,800 h, ~~with a degradation rate as low as 62.5 μV h^{-1}~~ with average cell voltage increased by 0.171 V, with a typical decay rate of 62.5 μV h^{-1}, demonstrating the great stability of $Y_{0.1}Ir_{0.2}Ru_{0.7}O_x$ from this perspective.

Comment 8:

The title claims a "universal design strategy," yet the data focus on Ru/Ir-based systems. Either provide supporting results across multiple catalyst families or narrow the title (for example, incorporate "Ru-based catalysts" into the title).

Response: We appreciate the Reviewer's reasonable suggestions. Following the Reviewer's suggestions and after our internal discussion, we agree that revising the title to "Directing Ru-based catalysts acidic oxygen evolution toward a universal dual-site pathway".

Comment 9:

The rationale for selecting Y, Sr, Sc and Mg should be clearly discussed. Explain why these elements were chosen over other possible dopants (electronic properties, ionic size, stability, prior literature precedents), and connect the choice to the mechanistic and structural design principles.

Response: We thank the Reviewer for his/her thoughtful consideration. As suggested, we have clarified our rationale for selecting Y, Sr, Sc, and Mg as representative elements to illustrate the catalyst design strategy for achieving such bond-length modulation as follows.

(i) Systematic distribution of ionic radii

The selected metals follow the trend of $Mg^{2+} < Sc^{3+} < Y^{3+} < Sr^{2+}$. Notably, their ionic radii, ranging from slightly smaller to ~1.5-2 times than of Ru^{4+} in rutile RuO_2. Importantly, their ionic radii (*Acta Crystallogr. A*, 1976, 32, 751) span a range from slightly smaller than to several times larger than that of Ru in rutile RuO_2 (0.67 Å) (Fig. 1d). This distribution is well suited to intuitively demonstrate how heteroatom M incorporation into the parent $RuIrO_x$ framework induces site-to-site distance compression, aligning with the manuscript's objective to visualize radius-driven structural effects. This deliberate selection enables a clear and intuitive demonstration of how heteroatom (M) incorporation into the parent $RuIrO_x$ framework compresses interatomic distances. As such, it directly supports the central objective of the manuscript: to visualize how ionic radius governs structural distortions in the catalyst lattice.

(ii) Low charge perturbation

While any dopant inevitably perturbs the local charge environment around Ru sites, Y, Sr, Sc, and Mg offer distinct advantages in their oxidized states: they are redox-

inactive and adopt either d^0 or near-closed-shell electronic configurations. As a result, they do not undergo valence-dependent ionic radius changes, nor do they introduce additional electronic degrees of freedom that could further complicate the local charge landscape (*J. Electrochem. Soc.,* 1984, 131, 290). These characteristics make these elements especially well-suited for studies aimed at isolating and systematically controlling interstitial distance effects.(iii) Compatibility with the framework structure

Notably, these elements have been reported to be incorporated into rutile RuO_2 or IrO_2 (*Nat. Catal.,* 2026, 1; *Nat Comm.,* 2025, 16, 1717; *Adv. Energy Mater.*, 2025, 2405657, etc.). While the objectives, compositions, macroscopic architectures, and synthetic protocols of our work differ from those studies, the demonstrated stability of Y, Sr, Sc and Mg in the acidic environments provided the rationale for their selection.

The above content and discussion have been incorporated into the revised manuscript. **(Page 4, Line 20)**.

Comment 10:

Pourbaix diagrams appear inconsistent or incomplete (Fig. 1g). Y and Ir species appear missing across the Pourbaix regions shown. Explain the meaning of the blue-filled regions and the mesh region in the figure. Verify the Pourbaix calculations and provide more detailed description (calculation conditions, concentration, pH range, potential range). Also check Fig. S20a for consistency.

Response: We thank the Reviewer for his/her careful and thoughtful attention to the Pourbaix diagrams. As this issue is closely related to the concern raised in Comment 17, we address both points together here to ensure a clear and coherent response.

(i) On Y and Ir species appear missing across the Pourbaix diagram

We would like to clarify that the decision to present the Pourbaix diagram of Ru, rather than those of Ir or Y, was made after careful consideration. First, the primary purpose of Pourbaix diagrams is to illustrate how the thermodynamic dissolution tendency of Ru in these Ru-based catalysts evolves with pH and potential after Y dopped. Specifically, the Pourbaix diagrams shown in the manuscript are intended to convey trends such as "the Ru component in $Ir_{0.2}Ru_{0.8}O_x$ is thermodynamically more corrosion-resistant than that in pristine RuO_2" or "$Y_{0.1}Ir_{0.2}Ru_{0.7}O_x$ exhibits higher thermodynamic stability than $Ir_{0.2}Ru_{0.8}O_x$. Second, Ru constitutes the majority of the metal species in $Y_{0.1}Ir_{0.2}Ru_{0.7}O_x$". The electronic and chemical environments of Ir and Y in this mixed oxide are no longer directly comparable to those in their respective

parent phases (e.g., Y_2O_3). Since the purpose of presenting the Pourbaix diagram is to provide readers with a qualitative understanding of the improved theoretical stability of $Y_{0.1}Ir_{0.2}Ru_{0.7}O_x$, constructing Pourbaix diagrams for the non-framework elements Ir and Y in the same manner would be neither reliable nor appropriate, and could risk conveying misleading interpretations. For these reasons, we chose to present only the Ru Pourbaix diagram in Fig. 1g.

(ii) On the meaning of the blue-filled regions and the mesh region in the figure

We apologize to the Reviewer for the insufficiently clear explanation of the illustrations in Fig. 1g in our initial submission. Below, we address each of the Reviewer's questions regarding Fig. 1g in detail.

The blue-filled regions in the Pourbaix diagram are referred to the "stable" or "protected" regions, indicating that RuO_2, $Ir_{0.2}Ru_{0.8}O_x$, or $Y_{0.1}Ir_{0.2}Ru_{0.7}O_x$ can thermodynamically remain in the rutile oxide form defined in the model. The upper potential limit of the blue-filled regions means the **Gibbs Free Energies** of RuO_2 and its dissolved species (RuO_4^{2-} or H_2RuO_5) are equal. The cross-hatched region illustrates the increase in the upper potential limit for maintaining the rutile phase stability of $Ir_{0.2}Ru_{0.8}O_x$ compared with conventional RuO_2, while the right-leaning hatched region indicates the further enhancement in the dissolution-resistant upper potential limit of $Y_{0.1}Ir_{0.2}Ru_{0.7}O_x$ relative to $Ir_{0.2}Ru_{0.8}O_x$. The above information has been incorporated into the figure caption of **Fig. 1g in the revised manuscript**.

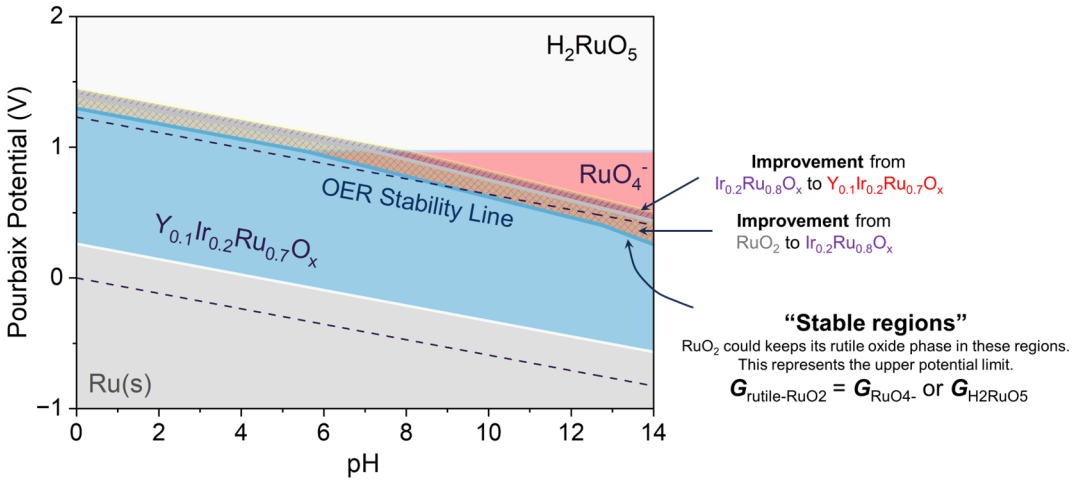

Figure. R7 Partial explanation of the overlapping Pourbaix diagram with shadows.

(iii) Verify the Pourbaix calculations and provide more detailed description (calculation conditions, concentration, pH range, potential range)

In practice, the calculated Pourbaix diagrams are indeed obtained by comparing the energies of different possible phases to determine their relative thermodynamic stability. To address the Reviewer's concerns, we have added the related clarification to the Methods section in the revised version **(Page 23, Line 1)**.

(iv) Check Fig. S20a for consistency

We carefully re-examined the original data used to construct Supplementary Fig. 20 and did not identify any unreasonable or inconsistent features. To further ensure data reliability, the Pourbaix diagram of $Y_{0.1}Ir_{0.2}Ru_{0.7}O_x$ has been included in Supplementary Fig. 20 in the revised manuscript with a consistent colour scheme.

(v) On "A higher potential of Pourbaix diagram should be performed to elucidate the thermodynamic stability of $Y_{0.1}Ir_{0.2}Ru_{0.7}O_x$"

We framed the primary purpose of the Pourbaix diagrams as quantifying how the addition of Y and Ir translates changes in model charge properties into altered dissolution tendencies. This is also the main reason we originally limited the Pourbaix diagrams to the -0.5 to 1.5 V range. The "potential" shown in a Pourbaix diagram reflects only the thermodynamics of valence changes or dissolution processes, and cannot be directly equated with the actual operating potential window of a PEMWE. Specifically, it is difficult to ignore the influence of polarization in a real PEMWE stack, the multiphase nature at interfaces, and the complex equilibria among multicomponent reactions, all of which prevent precise assignment of a single interfacial potential in the Pourbaix diagram that could be directly linked to dissolution. In the initial submission, the Pourbaix diagrams were therefore intended primarily to help readers understand how the thermodynamic changes induced by different element additions contribute to the improved stability of $Y_{0.1}Ir_{0.2}Ru_{0.7}O_x$.

Based on the Reviewer's suggestions, we have adjusted the potential range of the Pourbaix diagrams to "-1 to 2 V". The related changes and corrections have been updated in the revised manuscript **(Fig. 1g).**

Comment 11:

Fig. S22 indicates phase separation of Ir from Ru oxides. Discuss possible origins and implications for activity/stability.

Response: We sincerely thank the Reviewer for the insightful comment. No evidence of phase separation was observed in Fig. S22. RuO_2 and IrO_2 share nearly identical rutile structures and are well known to form homogeneous solid solutions across a wide

compositional range (*Chemistry of the Elements*, 2nd ed., Butterworth-Heinemann, 1997). Therefore, the reflections detected in Fig. S22 originate from the rutile-type, $Y_{0.1}Ir_{0.2}Ru_{0.7}O_x$ intermediate rather than from discrete RuO_2 or IrO_2 phases radii. In the original Supporting Information, the peaks near 28.5° and 35° were labelled as "RuO_2/IrO_2"; we have now carefully re-examined the assignments and corrected them to the corresponding (110) and (101) planes of the rutile-type intermediate. All updated annotations are included in the revised manuscript **(Supplementary Figures. 22c-24c)**.

Comment 12:

Based on the XRD analysis (Fig. S24c), is the sample a mixture of RuO_2/IrO_2 or a Y-Ru-Ir-O compound? The XRD pattern of $Ir_{0.2}Ru_{0.8}O_x$ should be given for comparison.

Response: The sample is not a physical mixture of RuO_2 and IrO_2. As clarified above, the observed reflections arise from the homogeneous rutile-type Y-Ru-Ir-O system. Following the Reviewer's suggestion, we have now added the XRD pattern of $Ir_{0.2}Ru_{0.8}O_x$ to the Supplementary Information for direct comparison (Fig. S24d in the Revised Supporting Information). This additional dataset further confirms that the diffraction features of the intermediate are consistent with those of a rutile-type solid solution rather than a mixture of individual oxides.

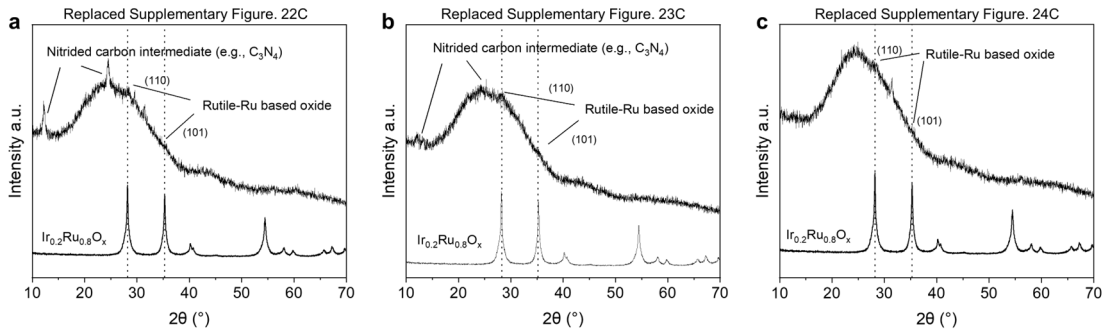

Figure. R8 Revised Supplementary Figs. 22c, 23c, and 24c. The updated XRD patterns are shown with each figure accompanied by a direct comparison to the XRD pattern of the finalized $Ir_{0.2}Ru_{0.8}O_x$ phase.

Comment 13:

The presence of Y reportedly shortens the Ru–Ru bond but lengthens the Ru–O bond. This appears contradictory from a bonding perspective — please explain the structural/chemical origin of this observation and, if possible, provide additional

analyses to reconcile these trends.

Response: We thank the Reviewer for his/her careful consideration and insightful interpretation of the structural details of the catalysts. We would like to clarify that the Ru-O components, each with uncorrelated degrees of freedom. Upon Y incorporation, a plausible mechanism is that the axially coordinated Ru-O bonds (two-fold coordination) undergo compression and consequent shortening due to lattice crowding, whereas the equatorially coordinated Ru-O bonds (four-fold coordination) are elongated as a result of framework expansion. Consequently, the experimentally observed Ru-O bond length appears as an overall "elongated" average value. This scenario is consistently supported by both the XAFS fitting results **(Table 3.)** and the DFT calculations (**Table 4** in the revised Supplementary Information).

Table 3. Ru K-edge EXAFS fitting results of $Y_{0.1}Ir_{0.2}Ru_{0.7}O_x$. (Supplementary Information).

	Shell	N^a	R (Å)	σ^2 (Å)	E^0 (eV)	R factor
Ru Foil	Ru-Ru	12*	2.675	0.00542	-0.033	0.0094
Rutile-RuO_2	Ru-O	6*	1.973	**0.00588**	-3.816	0.0144
	$Ru-Ru_1$	2*	3.187	0.00762		
	$Ru-Ru_2$	8*	3.541			
$Y_{0.1}Ir_{0.2}Ru_{0.7}O_x$	Ru-O	5.7	2.039	**0.01938**	-6.274	0.0190
	$Ru-Ru_1$	1.8	3.078	0.00653		
$Ir_{0.2}Ru_{0.8}O_x$	Ru-O	4.4	1.969	**0.00507**	-1.895	0.0142
	$Ru-Ru_1$	1.3	3.186	0.00618		
	$Ru-Ru_2$	9.0	3.534			

In Table 3 from the Supplementary Information in the initial submission, it can be observed that the Ru-O coordination σ^2 of $Y_{0.1}Ir_{0.2}Ru_{0.7}O_x$ increases abruptly from ~0.005 as in RuO_2 or $Ir_{0.2}Ru_{0.8}O_x$ to ~0.020. This is a typical manifestation of lattice distortion induced by compression, leading to a rearrangement of the fundamental rutile [RuO_6] octahedral framework. A similar phenomenon is also observed in the relaxed computational model of $YRuIrO_x$.

Table 4 The Average Ru-O bond lengths at several different positions after model relaxation (unit: Å)

	Ru-O short	*Ru-O medium*	*Ru-O long*
RuO_2 Model	/	1.978	/
$RuIrO_x$ Model	1.946	1.986	/
$YRuIrO_x$ Model	1.937	1.970, 1.991	2.028

In $YRuIrO_x$ model, the Ru–O bond lengths indeed exhibit a scenario, in which the compressed components are shortened while the radially oriented components are elongated, leading to a larger number of Ru-O bond-length parameters with independent degrees of freedom (*J. Synchrotron Radiat.,* 2005, 12, 537). This behaviour is in good agreement with the information obtained from the XAFS fitting. Moreover, such compression-induced, multi-coordination-averaged Ru-O bond-length features have also been reported in several recent studies (*J. Am. Chem. Soc*., 2025, doi: 10.1021/jacs.5c15759*; Nat. Commun*., 2025, 16, 6921), further supporting the validity of our interpretation. The above content and discussion have been incorporated into the revised manuscript (**Page 9, Line 3**).

Comment 14:

Y content values are missing in Fig. 2g.

Response: We thank the Reviewer for his/her kind reminder, and the sputtering information for each data point has been added Figure 2g in the revised version.

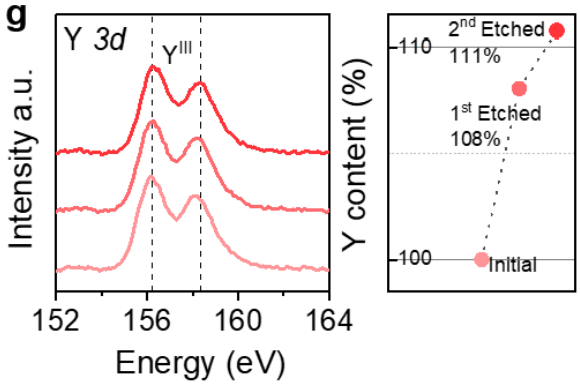

Fig. 2g Y *3d* depth-profiled XPS spectra of $Y_{0.1}Ir_{0.2}Ru_{0.7}O_x$ after successive etching.

Comment 15:

Update the comparison in the inset of Fig. 3f and Table 1 to include more recent Ir- and Ru-based OER catalysts published in high-impact journals to ensure a current and fair performance comparison.

Response: We thank the Reviewer for the insightful comment. As suggested, four new data points have been added in the Fig. 3f in the revised manuscript, and an additional fifteen entries have been included in the corresponding Table 1 in the revised Supporting Information.

Comment 16:

Supplementary Figure 13a shows that Sr also bridge adsorbs *OH and participates reaction. Does this structure influence the early intermediates such as *OH energy barriers, or still follow OPM?

Response: We thank the Reviewer for his/her careful attention to the details. In fact, Sr, like the other atoms introduced as dopants in the model, was not considered to participate in the reaction in our calculations. To avoid any potential misunderstanding, we examined and corrected similar images and added images showing the Sr-Ru-Ir model from different viewing angles above **Supplementary Figure 13a** in the revised Supplementary Information to clarify this point and address the Reviewer's concern.

Comment 17:

The potential window of Pourbaix diagram in Fig. 1g is of -0.5~1.5 V differs from those of $Ir_{0.2}Ru_{0.8}O_x$ and Ru (Supplementary Fig. 20). A higher potential of Pourbaix diagram should be performed to elucidate the thermodynamic stability of $Y_{0.1}Ir_{0.2}Ru_{0.7}O_x$, because practical application may operate at higher voltages.

Response: We thank the Reviewer for his/her accurate control over the details of the manuscript. Since this point pertains to the same Pourbaix diagram analysis addressed in Comment 7, it has already been fully covered in the combined response above. We have adjusted the potential window of **Fig. 1g** to be consistent with that shown in the Supplementary Information.

Comment 18:

References 29 and 30 do not mention the statement "…act as a negative charge centre,

protecting Ru from overoxidation" (Page 8 line 15). Please verify and correct this citation.

Response: We thank the Reviewer for his/her careful attention and kind reminder. We have replaced the inappropriate **ref.s 34 and 35** in the revised manuscript.

Comment 19:

The method used to calculate the S-number and the comparison with reported Ir- and Ru-based catalysts should be added for completeness.

Response: We thank the Reviewer for his/her suggestion.

The S-number was calculated as the number of evolved oxygen molecules divided by the number of dissolved site atoms (Ru/Ir). (*Nat. Catal.,* 2018, 1, 508). The amount of evolved oxygen was determined as:

$$n_{O_2} = Faradaic\ efficiency \times n_e\text{-}/4$$

where the Faradaic efficiency was assumed to be 100%. The numbers of dissolved Ru and Ir atoms were obtained by integrating the atom dissolution rate–time curves constructed from the ICP-MS results. We have additionally included several literature-reported S-numbers calculated using a methodology consistent with ours and provided a corresponding comparison.

Table 9. Benchmarking S-numbers of representative OER catalysts.

	$S\text{-number}_{Ru}$	$S\text{-number}_{Ir}$	$S\text{-number}_{PGM}$
$Y_{0.1}Ir_{0.2}Ru_{0.7}O_x$, 24h	1.06×10^7	1.14×10^8	9.70×10^6
$Y_{0.1}Ir_{0.2}Ru_{0.7}O_x$, 1000h	1.56×10^8	4.54×10^9	1.52×10^8
Crystal IrO_2[1]		10^6~10^7	
Ru-RuO_2-Sn[2]	6.7×10^6		
IrO_2(101) monolayer[3]		4.48×10^6	
$IrRuO_x/MnO_x$[4]	3.82×10^3	5.98×10^4	3.55×10^3

1. Geiger, S. *et al.* The stability number as a metric for electrocatalyst stability benchmarking. *Nat Catal* **1**, 508–515 (2018).

2. Song, Y. *et al.* Sub-4 nm Ru-RuO_2 Schottky Nanojunction as a Catalyst for Durable Acidic Water Oxidation. *J. Am. Chem. Soc.* **147**, 13775–13783 (2025).
3. Yang, D. *et al.* Single-faceted IrO2 monolayer enabling high-performing proton exchange membrane water electrolysis beyond 10,000 h stability at 1.5 A cm-2. *Nat Commun* **16**, 7236 (2025).
4. Kang, J. *et al.* Highly Active $IrRuO_x$ /MnO_x Electrocatalysts with Ultralow Anode PGM Demand in Proton Exchange Membrane Electrolyzers. *Advanced Energy Materials* 2405758 (2025) doi:10.1002/aenm.202405758.

This information has been added to the revised Supplementary Information (**Table 7**).

Comment 20:

The statement "…(0.1 mg_{Ir} cm^{-2} and 0.3 mg_{Ir} cm^{-2})…" on page 16 line 11 appears to be incorrect. Please revise accordingly.

Response: We thank the Reviewer for pointing out this oversight. The loading amount indicated on **Page 16, Line 23** has been corrected in the revised version. All similar labels throughout the manuscript have also been carefully rechecked and revised accordingly.

Comment 21:

The method for evaluating PEMWE activity in Fig. 3c should be described in detail, including electrochemical measurements and flow rates. In addition, the active area for evaluating activity and stability in PEMWE should also be declared.

Response: We thank the Reviewer for the constructive suggestions. As suggested, we have expanded Methods section associated with PEMWE to clearly describe the LSV measurement protocol and the durability testing procedures, including details such as flow rates, holding times at each LSV step, and the effective active area. The corresponding description has been added to the "Method" part of revised manuscript **(Page 22, Line 4)**.

The authors have addressed most of my previous concerns in the revised version. However, several issues still remain and should be further improved before the manuscript can be considered for publication.

We greatly appreciate the Reviewer's rigorous and insightful comments, which are of great value for us to clarify the remaining concerns and further improve the quality of this manuscript. Detailed point-by-point responses are provided below for your reference.

Comment 1:

The rationale for assuming Ru as the active site in the DFT calculations should be clearly explained in the revised manuscript, rather than being provided only as a brief statement. A more detailed justification is necessary to support this assumption.

Response: We thank the Reviewer for this meaningful comment. As suggested, the rationale for using Ru-centered adsorption sites in the DFT analysis has been clarified more explicitly in the revised manuscript. Ru-centered sites were selected as representative adsorption sites for the Ru-rich $Y_{0.1}Ir_{0.2}Ru_{0.7}O_x$ system, providing a consistent basis for evaluating the influence of Y and Ir incorporation on the local reaction energetics of the oxide framework. This treatment is also consistent with previous studies on Ru-Ir based oxides, where catalytic energetics are typically evaluated at Ru centers, with Ir serving mainly as an electronic or interfacial modulator (*Nat. Catal.* **2020**, 3, 516; *Nat. Commun.* **2024**, 15, 10315). This rationale has now been explicitly clarified in the revised manuscript (**Page 22, Line 27**).

Comment 2:

Second, the manuscript should include a clear statement, sufficient justification, and a detailed description of the procedure supporting the use of the Ru Pourbaix diagram to discuss the thermodynamic stability of $Y_{0.1}Ir_{0.2}Ru_{0.7}O_x$. The current explanation is insufficient to demonstrate the validity of this approach.

Response: Thank you for your constructive suggestion. The detailed rationale for adopting the Ru Pourbaix diagram to evaluate the thermodynamic stability of the $Y_{0.1}Ir_{0.2}Ru_{0.7}O_x$ catalyst is systematically summarized as follows. First, Y_2O_3 themself exhibits negligible intrinsic catalytic activity toward OER relative to the $Y_{0.1}Ir_{0.2}Ru_{0.7}O_x$ catalyst under typical electrochemical operating conditions. Second, the iridium oxides are generally acknowledged to possess much higher intrinsic structural stability than ruthenium oxides for OER (ref.s), thus, the overall thermodynamic stability of the

$Y_{0.1}Ir_{0.2}Ru_{0.7}O_x$ system is predominantly governed by the RuO_2-based matrix during practical OER operation. Third and most critically, Ru element constitutes the overwhelmingly dominant component in the $Y_{0.1}Ir_{0.2}Ru_{0.7}O_x$ after stability test (table 8). Consistently, representative XAFS characterizations further verify that the local coordination environment of $Y_{0.1}Ir_{0.2}Ru_{0.7}O_x$ closely matches that of RuO_2 (Figure 2j and Supplementary Figure 34). Collectively, considering the intrinsic material properties and absolute elemental content, Ru was selected as the primary reference element for the construction and analysis of the corresponding Pourbaix diagram, which can effectively simplify the system, clearly illustrate the key thermodynamic behaviour, and prevent misleading interpretation for readers.

As suggested by the Reviewer, we have added detailed clarifications in the revised manuscript, explicitly illustrating that the improved thermodynamic stability of $Y_{0.1}Ir_{0.2}Ru_{0.7}O_x$ is evaluated and validated based on the Ru Pourbaix diagram (**Page 7, Line 11**). More importantly, the complete underlying rationale, sufficient justification, and specific computational procedures have been fully supplemented and elaborated in the Methods section of the revised manuscript (**Page 23, Line 14**).

Comment 3:

Furthermore, the significant difference in elemental distribution clearly suggests possible phase separation between Ir and Ru oxides, with Ir appearing as aggregated bright-spot particles. The authors should discuss the possible origin of this observation and its implications for catalytic activity and stability.

Response: We thank the Reviewer for the insightful comment. We would like to clarify that the TEM images in Supplementary Figures 22 to 24, referenced by the Reviewer correspond to intermediate stages of the synthesis process at 1 and 5 min, not the final catalyst obtained after 100 min of thermal treatment at 500 °C. These images are included to illustrate the structural evolution during the carbon-templated formation process. However, as you can see upon close inspection, the Ru, Ir, and Y elements are co-located. This coexistence paves the way for the formation of a catalyst with uniform elemental dispersion after calcination at 500 °C for 100 min.

In fact, the typical catalyst of $Y_{0.1}Ir_{0.2}Ru_{0.7}O_x$ is more likely to form a homogeneous phase rather than a phase-separated system, being demonstrated by other characterization techniques that are more sensitive to local structure. For example, Fig. 2j shows Ru K-edge XAFS features that differ clearly from those of RuO_2 and Ru foil,

indicating the presence of Ru-O-M coordination. Furthermore, the AC-TEM images with much higher magnification reveal a structurally disordered yet spatially uniform nanosheet morphology (Fig. 2a-d). In addition, post-test analyses after both the three-electrode and PEMWE measurements show that the catalyst remains structurally intact with uniform elemental dispersion, further supporting its structural stability (Supplementary Figure 59). The relevant discussion has been revised and highlighted accordingly in the revised manuscript, with the structural stability of the catalyst now emphasized more clearly (**Page 7, Line 25**).

Comment 4:

Moreover, due to the relatively weak diffraction intensity, the XRD patterns presented in the manuscript are insufficient to convincingly support the claim that the sample forms a homogeneous Y-Ru-Ir-O compound, rather than a mixture of RuO_2 and IrO_2 phases.

Response: We thank the Reviewer for this comment. In the revised manuscript, we have clarified the scope of the XRD analysis and revised the related discussion to avoid overstating the structural implication of these data. As RuO_2 and IrO_2 exhibit very similar rutile-type diffraction features with closely matched lattice parameters, XRD patterns alone is, of course, insufficient to provide definitive evidence to distinguish a homogeneous phase from subtle RuO_2/IrO_2 phase separation. As the Reviewer noted, resolving such structural ambiguity typically requires complementary techniques that are sensitive to local coordination environments. For the intermediate samples (Supplementary Figures 22 to 24), the XRD results are used only to indicate the formation and evolution of oxide-related species, instead of serving as evidence for a homogeneous ternary phase.

In this context, TEM, XAFS, and SAED characterizations (Figs. 2a to d, Figs. 2i and j, Supplementary Figure 28) and the relevant description collectively support that the final $Y_{0.1}Ir_{0.2}Ru_{0.7}O_x$ structure exhibits good phase homogeneity. In the section describing intermediates, we have added clarifications and removed statements that could potentially lead to ambiguity (note after **Supplementary Figure 24**).

The authors have further addressed my comments; however, the discussion based on the Ru Pourbaix diagram to evaluate the thermodynamic stability of $Y_{0.1}Ir_{0.2}Ru_{0.7}O_x$ remains inappropriate. In particular, some statements are misleading. A Pourbaix diagram is fundamentally used to assess thermodynamic stability and possible phase stability domains under electrochemical conditions, not catalytic activity. Therefore, the statement that "Y_2O_3 themself exhibits negligible intrinsic catalytic activity toward OER relative to the $Y_{0.1}Ir_{0.2}Ru_{0.7}O_x$ catalyst under typical electrochemical operating conditions." is conceptually incorrect in this context. Thermodynamic stability analysis cannot be used to justify catalytic activity comparisons.

Response: Many thanks for your meticulous and rigorous comment. The potentially misleading statements you identified have been removed in the revised manuscript. The summary of the Pourbaix computational strategy provided in the Methods section has also been updated. Ambiguous descriptions have been removed, and the newly added multicomponent Pourbaix analysis has been incorporated to provide a more complete and transparent description of the calculation procedures (**Page 23, Line 22**).

More importantly, the stability of Y-containing species is not properly addressed. Y_2O_3 (or Y species in the oxide lattice) may undergo dissolution or phase instability under operating OER conditions, which could significantly affect catalyst durability. This aspect appears to be overlooked. Accordingly, the authors are encouraged to construct and analyse the Pourbaix diagram of $Y_{0.1}Ir_{0.2}Ru_{0.7}O_x$, rather than relying solely on the Ru Pourbaix diagram, which does not adequately represent the multicomponent system.

Response: Thank you for the sincere comments. A full-composition Pourbaix diagram that includes Y-containing species in the oxide lattice has been added as Supplementary Figure 20 in the revised manuscript. In this analysis, a more comprehensive set of potentially relevant phases was considered, including $Y_{0.1}Ir_{0.2}Ru_{0.7}O_x$, RuO_2, IrO_2, Y_2O_3, $Y_2Ru_2O_7$, $Y_2Ir_2O_7$, RuO_4, YH_2, and $IrRu_3$, together with the effects of species stoichiometry and concentration. The complete and corrected computational procedure for the Pourbaix analysis has also been incorporated into the revised manuscript (**Page 23, Line 22**).

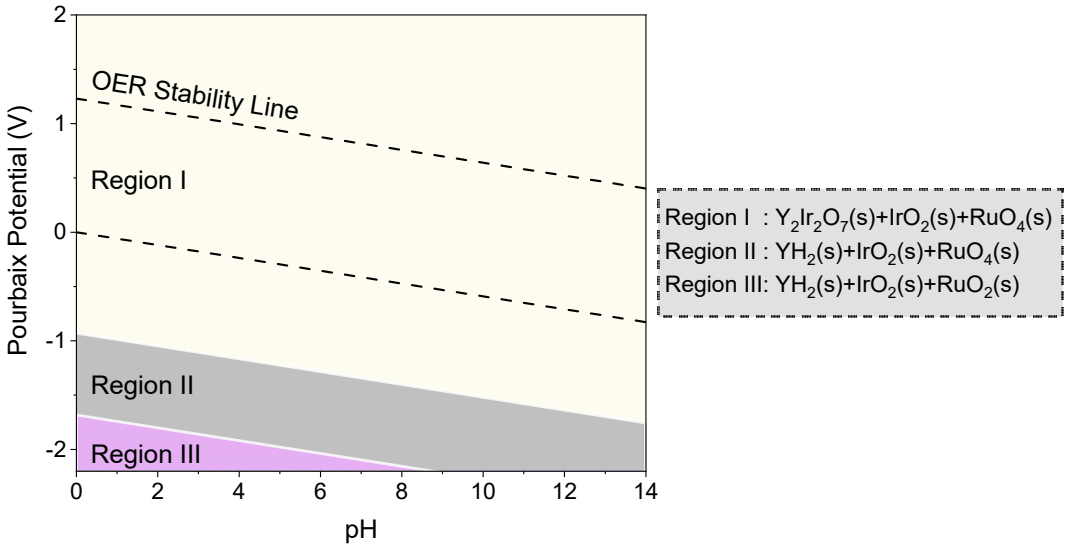

Supplementary Figure 20. Pourbaix diagram shows the thermodynamic stability regions of Y-, Ir-, and Ru-containing species in $Y_{0.1}Ir_{0.2}Ru_{0.7}O_x$.

As the Pourbaix diagram represents only the thermodynamic comparison of Gibbs free energies among competing phases, the multicomponent $Y_{0.1}Ir_{0.2}Ru_{0.7}O_x$ phase does not appear as the thermodynamically most stable species within the OER-relevant region (Region I). Likewise, in the highly reducing potential range below the HER region (Regions II and III), thermodynamically stable alloy or hydride phases are predicted to form. Since these regions lie well outside the practical OER operating window, they are not discussed further in this work.

In Supplementary Figure 20, the thermodynamically stable Y-containing species within the OER-relevant region is predicted to be $Y_2Ir_2O_7(s)$, indicating that Y is thermodynamically retained within Y-containing oxide phases under these conditions. In contrast, the Ru component exhibits a greater thermodynamic tendency toward oxidation and dissolution within this potential range. Taken together, the multicomponent Pourbaix analysis suggests that Y incorporation does not introduce a preferential thermodynamic driving force for Y dissolution. Complementarily, the Ru-centred Pourbaix analysis (Fig. 1g) indicates a reduced Ru-related dissolution tendency relative to the reference systems.

In light of these considerations, we have revised the corresponding discussion of the Pourbaix analysis in the main text and further incorporated the implications of the full-composition Pourbaix diagram (**Page 7, Line 10**).

We sincerely thank you for the substantial effort and thoughtful comments provided throughout the review process. The suggestions and critiques offered during multiple rounds of revision have been instrumental in improving the quality, clarity, and rigor of this manuscript. Seizing this final opportunity for revision, we have exercised utmost care and made every possible effort to refine our work. We greatly appreciate your time, expertise, and commitment to maintaining high scientific standards, and hope that the revised manuscript satisfactorily addresses the concerns and meets your expectations.

Reviewer #4

I appreciate the authors' efforts in revising the manuscript. The removal of the misleading statements regarding catalytic activity, together with the inclusion of a multicomponent Pourbaix analysis that explicitly considers Y-containing phases, has substantially improved the discussion and addressed my previous concerns. Since the authors still keep the initial Pourbaix analysis in Fig. 1g, I believe, that several aspects of the interpretation would benefit from more cautious wording to ensure that the conclusions remain fully consistent with the scope and limitations of the Pourbaix analysis.

According to Supplementary Figure 20, the thermodynamically stable phase under OER-relevant conditions is predicted to be $Y_2Ir_2O_7$, rather than the synthesized $Y_{0.1}Ir_{0.2}Ru_{0.7}O_x$, suggesting that the catalyst is thermodynamically metastable. Therefore, the statement that "Y incorporation does not introduce a preferential thermodynamic driving force for Y dissolution" would benefit from more careful qualification. The Pourbaix analysis identifies the equilibrium phase assemblage with the lowest Gibbs free energy but does not demonstrate that Y remains incorporated within the original catalyst lattice during operation. Likewise, the predicted equilibrium of $Y_2Ir_2O_7$ and RuO_4 indicates that phase reconstruction is thermodynamically favourable. Accordingly, the conclusions regarding catalyst durability should continue to rely primarily on the experimental stability results, with the Pourbaix analysis providing qualitative thermodynamic insight. Moreover, please make sure RuO_4 in Supplementary Figure 20 is solid species since RuO_4 appears as dissolved species in Fig. 1g. In addition, I suggest a minor revision to the description of Fig. 1g. Based on the computational methodology and the authors' explanation, Fig. 1g represents a Ru-centred Pourbaix analysis of Ru-related phases under different chemical environments, rather than a true Pourbaix diagram of $Y_{0.1}Ir_{0.2}Ru_{0.7}O_x$. If the authors would like to keep Fig. 1g as it is, revising the figure caption and corresponding discussion to reflect this distinction would improve consistency with the methodology and avoid confusion with the multicomponent Pourbaix analysis presented in Supplementary Figure 20. These minor clarifications would further strengthen the scientific rigor of the manuscript.

Response: We sincerely thank the Reviewer for the insightful comments and the careful attention devoted to the details of our manuscript. We agree with your assessment

regarding the thermodynamic metastability of the catalyst and the distinction between the two types of Pourbaix analyses.

We acknowledge that the multicomponent Pourbaix analysis (Supplementary Figure 20) predicts $Y_2Ir_2O_7$ as the equilibrium phase, suggesting that the synthesized phase is thermodynamically metastable with respect to the calculated equilibrium assemblage. Accordingly, we have revised the manuscript to qualify our statements, emphasizing that the experimental stability results are the primary basis for our conclusions on durability, while the Pourbaix analysis serves to provide qualitative thermodynamic insights **(Page 6, Line 5).**

The initial "RuO_4(s)" label in Supplementary Figure 20 stems from the fact that the full-composition Pourbaix analysis is constructed from phases explicitly included in the computational database. As suggested and after careful consideration, we have revised the labelling scheme and adopted a consistent nomenclature throughout the revised manuscript by uniformly designating dissolved Ru species according to their oxidation states, thereby avoiding potential confusion arising from database-specific phase representations **(Page 19, Line 14).**

We agree your suggestion to clarify the nature of Fig. 1g. In the previous Ru-based Pourbaix analysis, the results identify the thermodynamically most stable reference species under given conditions, rather than the exact species present experimentally. To avoid confusion with the equilibrium phases in Supplementary Figure 20 and to prevent misinterpretation of species like "H_2RuO_5(aq)", we have made the following revisions.

(1) The caption of Fig. 1g has been revised to "The pH-potential diagram from the Ru-based Pourbaix analysis of $Y_{0.1}Ir_{0.2}Ru_{0.7}O_x$" in the revised version to accurately reflect its methodological scope.

(2) In the revised version, dissolved Ru species with different oxidation states have been uniformly relabelled as "dissolved Ru(VI), Ru(VII), or Ru(VIII)". This avoids implying the existence of specific thermodynamic reference species (e.g., H_2RuO_5) that may not correspond to experimentally distinguishable dissolved species.

The authors have addressed most of my previous concerns in the revised version. However, several issues still remain and should be further improved before the manuscript can be considered for publication.

The rationale for assuming Ru as the active site in the DFT calculations should be clearly explained in the revised manuscript, rather than being provided only as a brief statement. A more detailed justification is necessary to support this assumption.

Second, the manuscript should include a clear statement, sufficient justification, and a detailed description of the procedure supporting the use of the Ru Pourbaix diagram to discuss the thermodynamic stability of Y0.1Ir0.2Ru0.7Ox. The current explanation is insufficient to demonstrate the validity of this approach.

Furthermore, the significant difference in elemental distribution clearly suggests possible phase separation between Ir and Ru oxides, with Ir appearing as aggregated bright-spot particles. The authors should discuss the possible origin of this observation and its implications for catalytic activity and stability.

Moreover, due to the relatively weak diffraction intensity, the XRD patterns presented in the manuscript are insufficient to convincingly support the claim that the sample forms a homogeneous Y–Ru–Ir–O compound, rather than a mixture of RuO2 and IrO2 phases.